PAP 12

DETERMINATION OF PRESSURE-CONTROLLED PROFILES FOR MORNING-GLORY SPILLWAYS

By

W. E. Wagner

Engineer, Bureau of Reclamation
Design and Construction Division
Denver, Colorado

A paper for the
Summer Convention, ASCE,
Denver, Colorado, June 1952

DETERMINATION OF PRESSURE-CONTROLLED PROFILES FOR MORNING-GLORY SPILLWAYS

By

W. E. Wagner*

INTRODUCTION

With the increasing use of the morning-glory or shaft spillway, there is a general need for additional data to aid the hydraulic engineer in designing a morning-glory for the many conditions encountered in the field. Some of the problems which must be solved are the size and shape of the overflow section; the size of the shaft; the degree of curvature of the bend connecting the shaft with the horizontal tunnel; and the method of stilling the high velocity flow before it enters the river channel below the dam. Each of these problems is important and requires careful consideration. This paper deals with the first problem: that of determining the size and shape of the overflow section which will pass the required quantity of water at the desired head and which will provide pressures on the morning-glory profile which are above the cavitation range. To find a solution to this design problem, a circular weir was constructed and tested in the Hydraulic Laboratory of the Bureau of Reclamation. The sharp-crested weir used in these studies was circular in plan and 20 inches in diameter. Flow passing over the weir springs clear at the sharp edge and the lower trace of the nappe indicates the shape of the morning-glory surface for given conditions of head above the crest, approach depth, and pressure beneath the nappe.

Discharge coefficients and the shapes of the upper and lower nappe surfaces, fully aerated, were obtained for three approach depths; namely 20, 3, and 1-1/2 inches below the crest of the weir. The comparatively shallow 3- and 1-1/2-inch depths were chosen to assure a measurable effect on the discharge and nappe shapes. In addition, the effect on the nappe shape of reducing the pressure by removing air from the space under the nappe was studied. The reduced pressure studies were made for negligible velocity of approach using the 20-inch approach depth. Data were taken only on an intermediate range of discharges where a stable jet could be maintained since at both higher and lower discharges pulsations in the nappe made measurements impossible.

The following discussion includes a description of the test equipment and the procedures followed in developing a method for determining the shape of the overflow section of a morning-glory spillway. Finally the experimental results are applied to a working model of the spillway for Hungry Horse Dam.

*Engineer, Bureau of Reclamation, Design and Construction Division, Denver, Colorado.

Most of the material contained herein was submitted to the University of Colorado as a thesis in partial fulfillment of the requirements for the degree, Master of Science, in 1952.

SYMBOLS

The following is a list of symbols used in this paper. Reference is made to Figure 1.

Q = discharge in cubic feet per second

h_s = observed head on weir measured 22 inches from weir crest, feet

V_a = average velocity of approach computed 22 inches from the weir crest, feet per second

h_a = average velocity head of approach in $h_a = \frac{V_a^2}{2g}$, feet

$H_s = h_s + h_a$ = total head above weir crest, feet

E = maximum rise of lower nappe surface above sharp crest of weir, feet

h_o = observed head above high point on lower nappe surface, feet

$H_o = h_o + h_a$ = total head above high point on lower nappe surface, feet

R = radius of sharp crest of test weir, feet

$L = 2\pi R$ = crest length of circular test weir, feet

P = depth of approach floor below weir crest, feet

h_p = observed pressure, below atmospheric, in air chamber under the nappe, feet of water

$C = \frac{Q}{LH_s^{3/2}}$ = coefficient of discharge for test weir

X = horizontal coordinate, origin at weir crest, negative upstream and positive toward center of test weir, feet

Y = vertical coordinate, positive above and negative below crest of weir

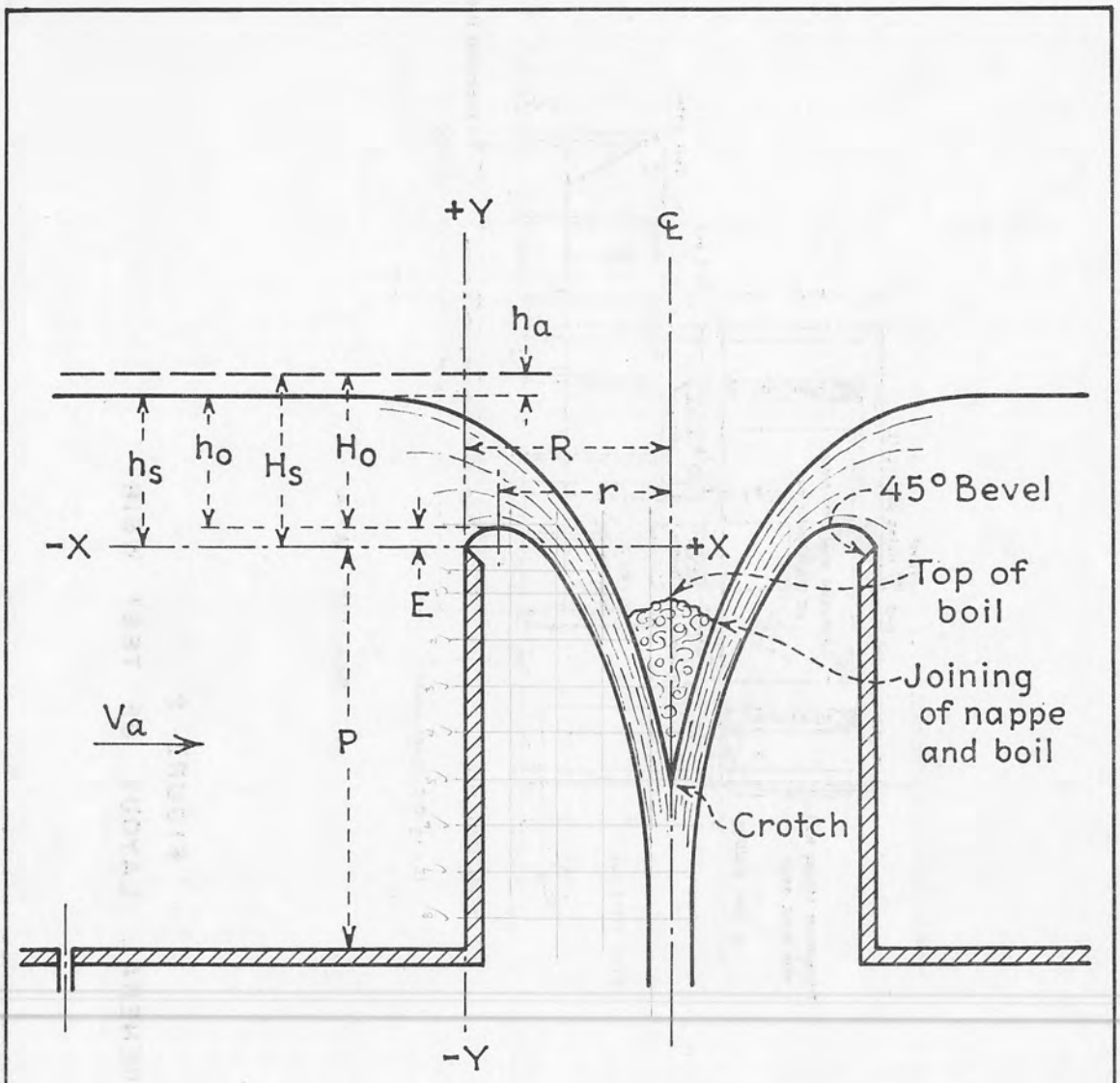

FIGURE 1. - PRINCIPAL ELEMENTS OF CIRCULAR WEIR

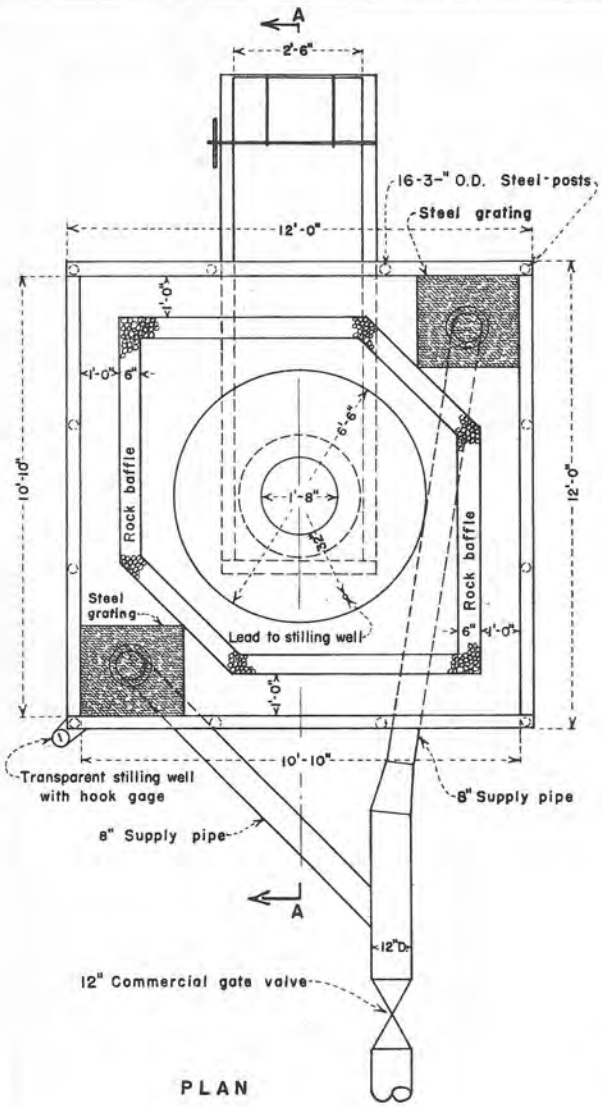

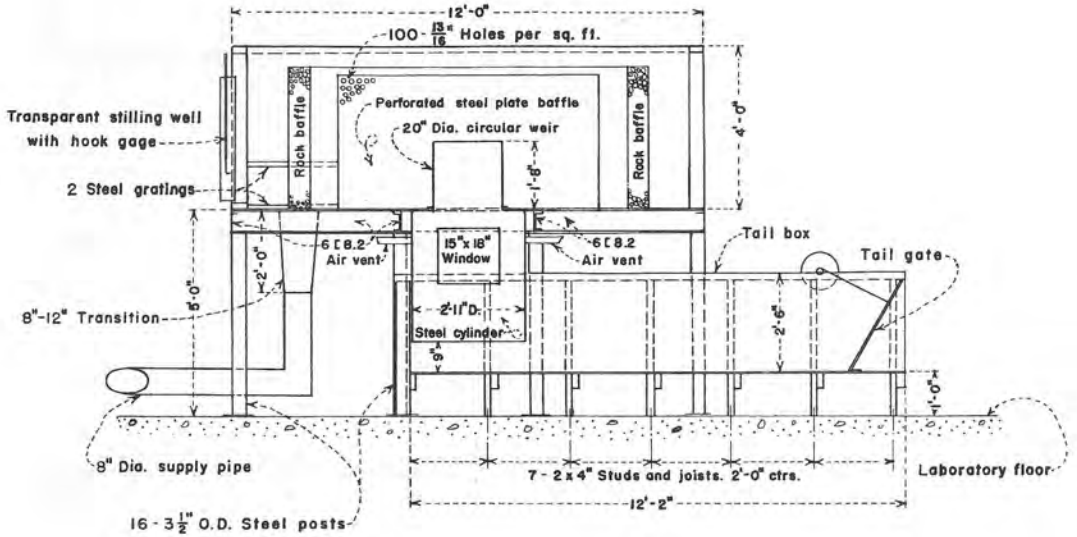

SECTION A - A

FIGURE 2

GENERAL LAYOUT OF TEST WEIR

322

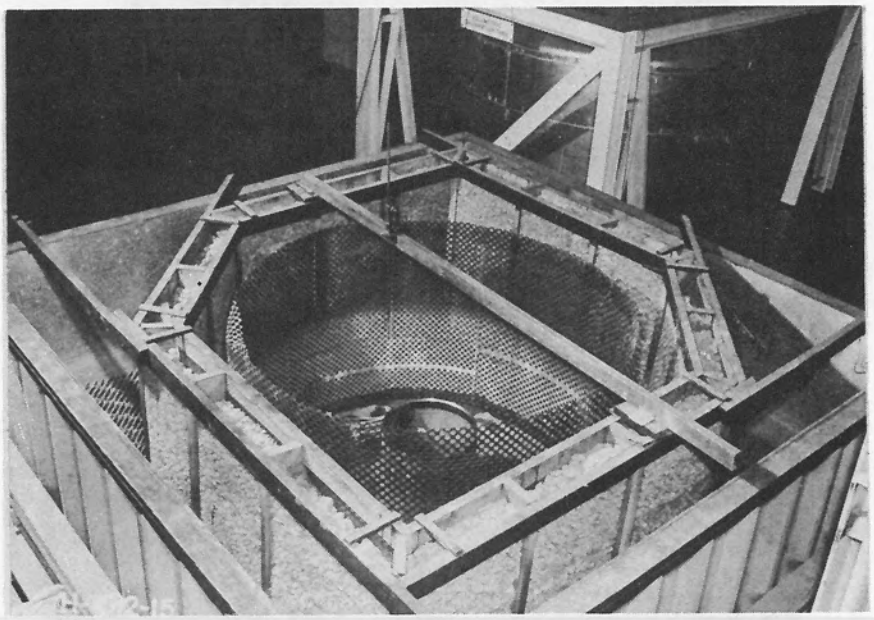

Figure 3. General view of headbox containing test weir

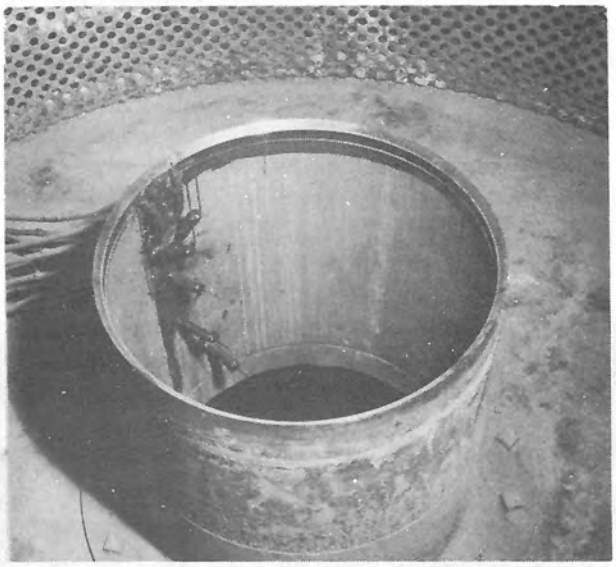

A. Test weir showing probes for outlining lower nappe surface

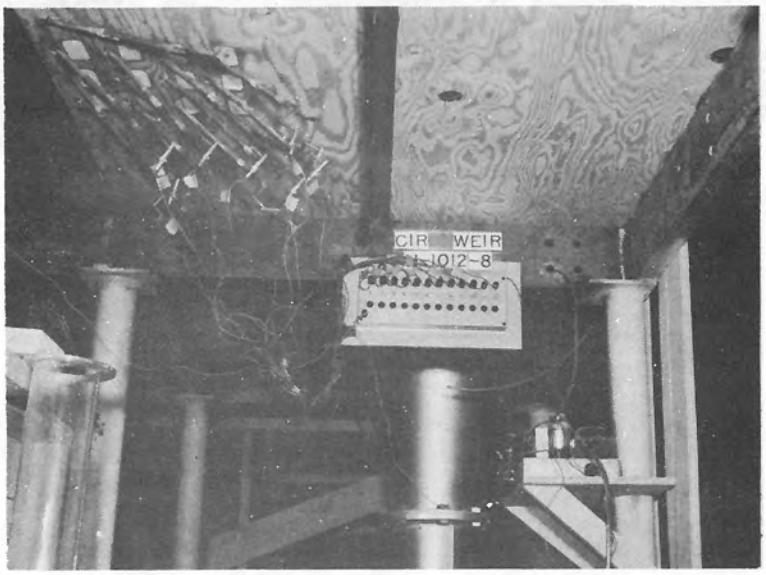

B. Probe adjusting screws and electronic contact indicator

Figure 4. Probes and electronic contact indicator

TEST EQUIPMENT

The Test Weir

The general arrangement of the test weir is shown in Figures 2 and 3. The test weir was fabricated from a 20-inch length of seamless steel pipe, 20-inch outside diameter with 1/2-inch wall. The outside surface of one end of the cylinder was machined to form a true circle, 1.6593 feet in diameter. A 45° bevel was then machined from the inner face until a knife edge was formed by the intersection of the 45° bevel and the outer machined surface. A steel flange, for bolting the test weir to the floor of the head box was welded to the other end of the pipe.

The head box, 12 feet square with 4-foot side walls (outside dimensions), was elevated to a height 5 feet above the laboratory floor. The construction of the testing box and weir was sufficiently strong to maintain the weir in a level position when the head box was full of water.

Water was supplied to the head box through two 8-inch inlets which terminated in the floor at diagonal corners of the testing box. Several precautions were taken to assure that the water approached the weir radially and uniformly. A 6-inch-thick baffle, containing 3/4- to 1-inch gravel was placed approximately 1 foot from the side walls of the head box, Figure 3. Two steel gratings were placed over each inlet to reduce the boil and distribute the inflowing water between the side walls of the head box and the gravel baffle. To quiet the flow further before passing over the test weir, a perforated cylinder was placed between the gravel baffle and the weir. The perforated cylinder, 6-1/2 feet in diameter and 4 feet high, was made from a 12-gage steel plate punched with one hundred 13/16-inch-diameter holes per square foot.

Discharge Measurements

The discharge over the circular weir was measured by either a 4-, 6-, 8-, or 12-inch commercial venturi meter, depending upon the discharge required for the particular test. All the laboratory venturi meters were accurately calibrated by means of a volumetric tank.

Water-surface Gages

Head gage. The head, h_s, on the test weir was measured by a hook gage mounted in a stilling-well located at the side of the head box. A 3/16-inch-inside-diameter rubber tube connected the stilling-well to the head box at a point 22 inches from the sharp crest of the test weir.

Upper surface gage. Profiles of the upper water surface over the test weir were taken with a point gage mounted on an aluminum channel. Sufficient readings were observed to establish a smooth curve describing the shape of the upper nappe surface. The zero of these gages was checked before and following each set of runs.

Lower surface gage. To determine the shape of the lower nappe surface, the profile first was outlined by means of 13 wire probes extending through the wall of the weir and spaced at different intervals below the crest of the test weir, Figure 4A. The end of each probe was positioned along the nappe by screwing the probe toward the sheet of water until contact was made with the lower nappe surface. Contact of the probe with the nappe was indicated by a 6-volt bulb which lighted when the end of the probe barely touched the lower nappe surface. Figure 4B shows the probe adjusting screws and the electronic contact indicator.

The coordinates of the points of each probe, outlining the lower nappe profile, were measured with a specially designed point gage, Figure 5. The gage consisted of a horizontal beam, which rested on the crest of the test weir, and a vertical bar mounted in a carriage which rode along the horizontal bar. The lower end of the vertical bar was fitted with a point for positioning the gage at the end of the wire probe. The point of the gage was positioned over the probe by moving the carriage horizontally along the beam and lowering the vertical bar until the point contacted the probe.

Means of Altering Velocity of Approach

The test weir was constructed with its crest 20 inches from the floor of the head box and most of the data were obtained with this approach depth. However, to determine the effect of velocity of approach on the coefficient of discharge and the nappe shapes, experiments also were made with the approach depth 3 and 1-1/2 inches below the weir crest. The approach depth, P, was changed by placing a horizontal false floor between the upstream face of the weir and the perforated cylinder, Figure 6.

With the approach depth 20 inches below the weir crest the velocity head, h_a, was less than 0.0005 foot for $\frac{H_s}{R}$ ratios under 0.60 and reached a maximum of 0.0007 foot for an $\frac{H_s}{R}$ ratio of 2.00. Therefore, the velocity head was considered negligible for data obtained with the 20-inch approach depth. For the 3-inch approach depth, the velocity head varied from 0.001 to 0.004 foot and 0.001 to 0.005 foot for the 1-1/2-inch approach depth.

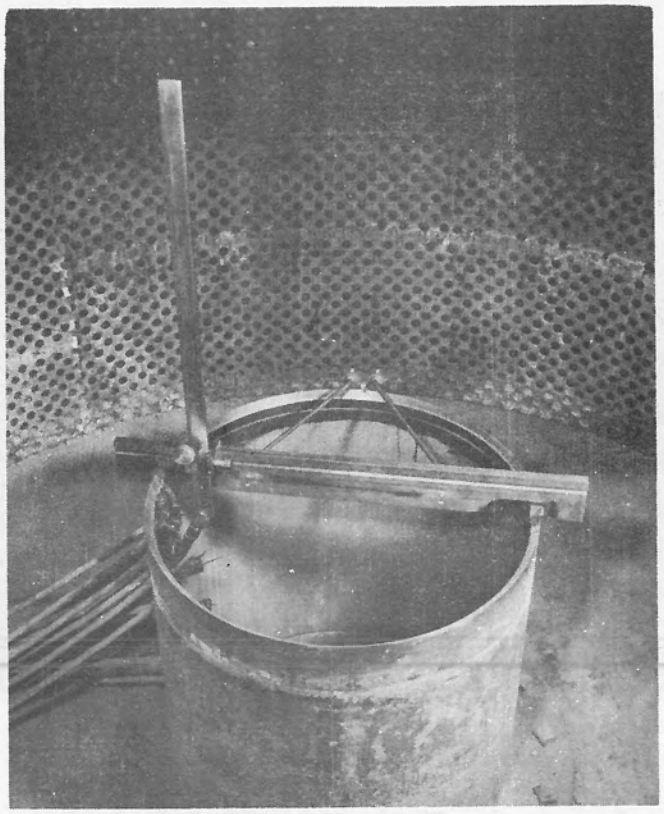

Figure 5. Special point gage
for measuring coordinates
of probes

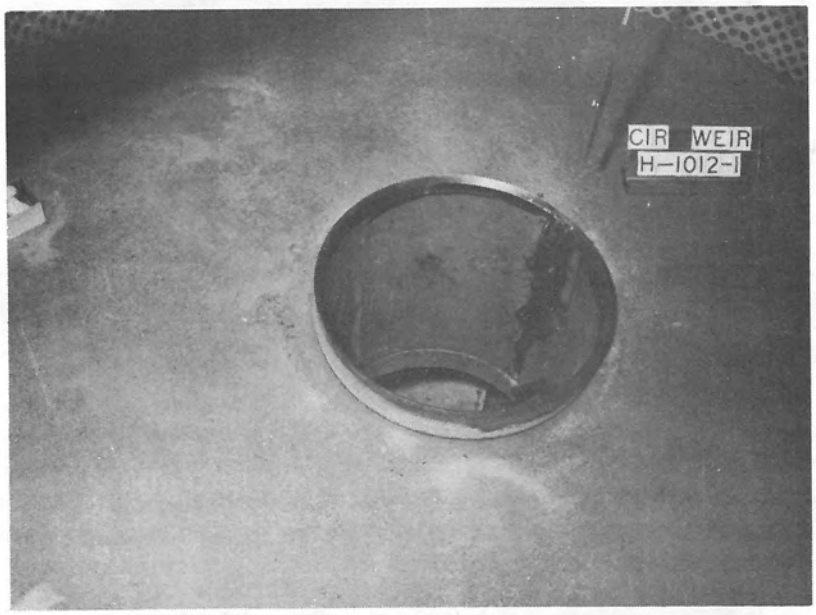

Figure 6. Test weir with 3-inch approach depth

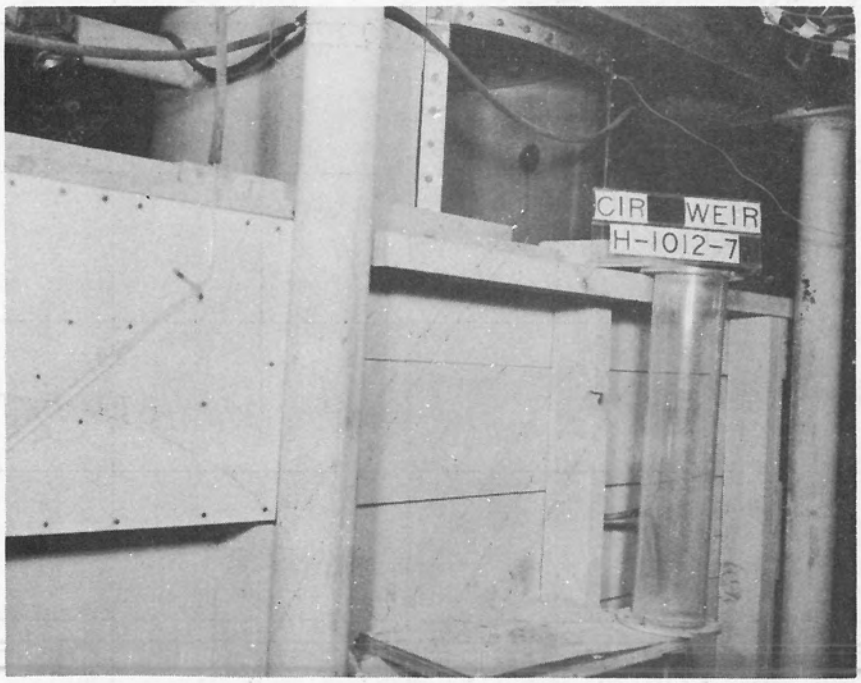

Figure 7. Tailbox and cylinder for reducing the pressure under the nappe

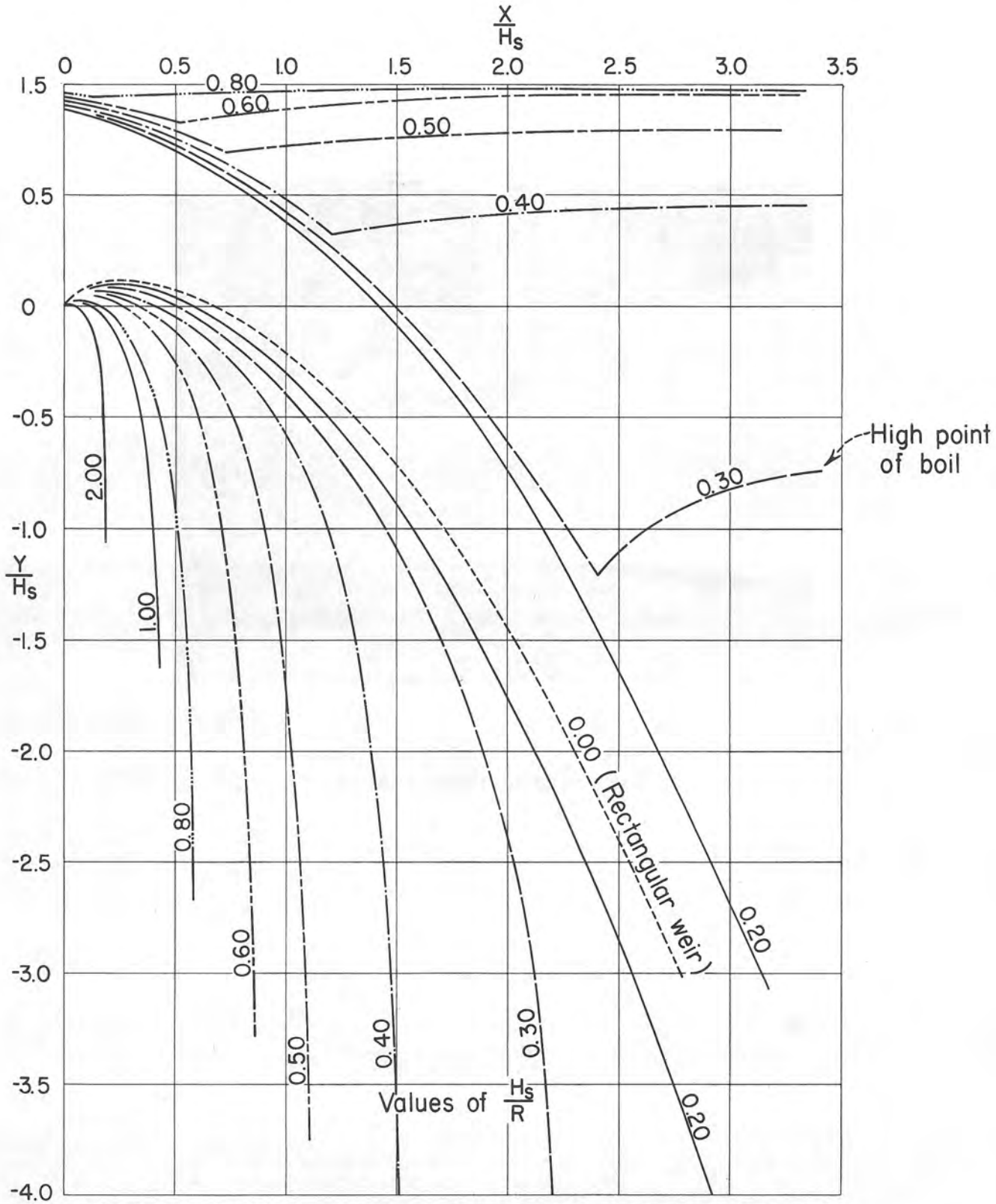

FIGURE 8-TYPICAL UPPER AND LOWER NAPPE SURFACES
(Aerated nappe and negligible approach velocity)

Means of Reducing the Pressure Under the Nappe

To study the effect of subatmospheric pressures under the nappe, a sheet-metal cylinder, 35 inches in diameter, 3 feet long and flanged at one end, was bolted to the underside of the head box concentric with the test weir, Figure 7. The lower end of the cylinder was approximately 9 inches from the floor of the tail box. By means of a tail gate, the water surface in the tail box could be raised to submerge the end of the cylinder, thus sealing the air chamber between the falling jet and the cylinder walls. The jet, in falling, pumped some of the air from the chamber and reduced the pressure in the space beneath the nappe. Two vents, each 3 inches in diameter and equipped with gate valves, were placed in the wall of the cylinder. By controlling the amount of air entering the chamber, a fairly stable pressure could be maintained under the nappe. For the lower pressures and discharges, it was found necessary to connect a vacuum line to the chamber to secure the desired pressure.

The pressure in the chamber was measured by a differential U-tube manometer filled with water. The legs of the manometer were tilted at 45^{o} to permit reading of the differential pressure to 0.001 foot.

INTERPRETATION OF RESULTS

Discharge Coefficient

The flow over a circular weir may be classified as either free or submerged. For free flow, the discharge characteristics are similar to those for the rectangular weir, where $Q = CLH_S^{3/2}$. Thus, the theoretical discharge is directly proportional to the three-halves power of the head, H_S, on the weir.

When the discharge increases until the water surface is practically level above the weir, the weir becomes an orifice and the theoretical discharge follows the form $Q = C_O A_O \sqrt{2gH_S}$. For orifice flow, an increase in head results in a very limited increase in discharge since the theoretical discharge is then proportional to the square root of the head. For partial submergence, the discharge coefficient, C or C_O, changes more rapidly with head and the discharge characteristics follow neither the orifice nor weir formulas.

Since the point where weir flow ends and orifice flow begins is difficult to define, and to simplify the method of expressing the coefficient of discharge, the weir formula, $Q = CLH_S^{3/2}$, was used to

compute the discharge coefficients throughout the range of testing. The weir formula was chosen because most morning-glory spillways are designed for free flow.

Nappe Profiles

From the laws of similitude, it can be shown that the profiles of a sheet of water flowing over any two sharp-crested, circular weirs with aerated nappe and negligible velocity of approach are similar if the respective ratios of the head, H_s, to the radius, R, of the weirs are the same. Thus, by expressing the X and Y coordinates of the nappe surfaces and the radius of the weir in terms of H_s, the results are in dimensionless form and the nappe shape for any head and radius of weir can be determined. Camp and Howe [1] found in their experiments on three weir arcs of different radii that "nappe profiles plotted in terms of these dimensionless coordinates proved to be practically identical for runs having the same ratio of head to diameter of weir arch except in those runs in which the head was so low that the nappe adhered to the crest."

This was the method used in plotting the upper and lower surface of the nappe. The X and Y coordinates of the nappe surfaces, obtained from the test weir, were divided by H_s, plotted with as many as three runs for each value of $\frac{H_s}{R}$, and an average line drawn through the points. This was done on a scale too large for reproduction in this paper. However, Figure 8 is representative of the shapes of the curves. In place of the curves, the $\frac{X}{H_s}$ and $\frac{Y}{H_s}$ coordinates are tabulated in Tables 1 through 6.

ANALYSIS OF RESULTS

Discharge Coefficients

The coefficient of discharge, C, versus the dimensionless ratio $\frac{H_s}{R}$ for three approach depths is plotted in Figure 9. In each case, the lower surface of the nappe was open to the atmosphere and fully aerated. The lower curve, designated the Base Curve, shows the discharge coefficient for $\frac{H_s}{R}$ ratios between 0.20 and 2.00 with the approach floor 20 inches below the weir crest, or with negligible velocity of approach.

1/ Numbers refer to list of references in Bibliography.

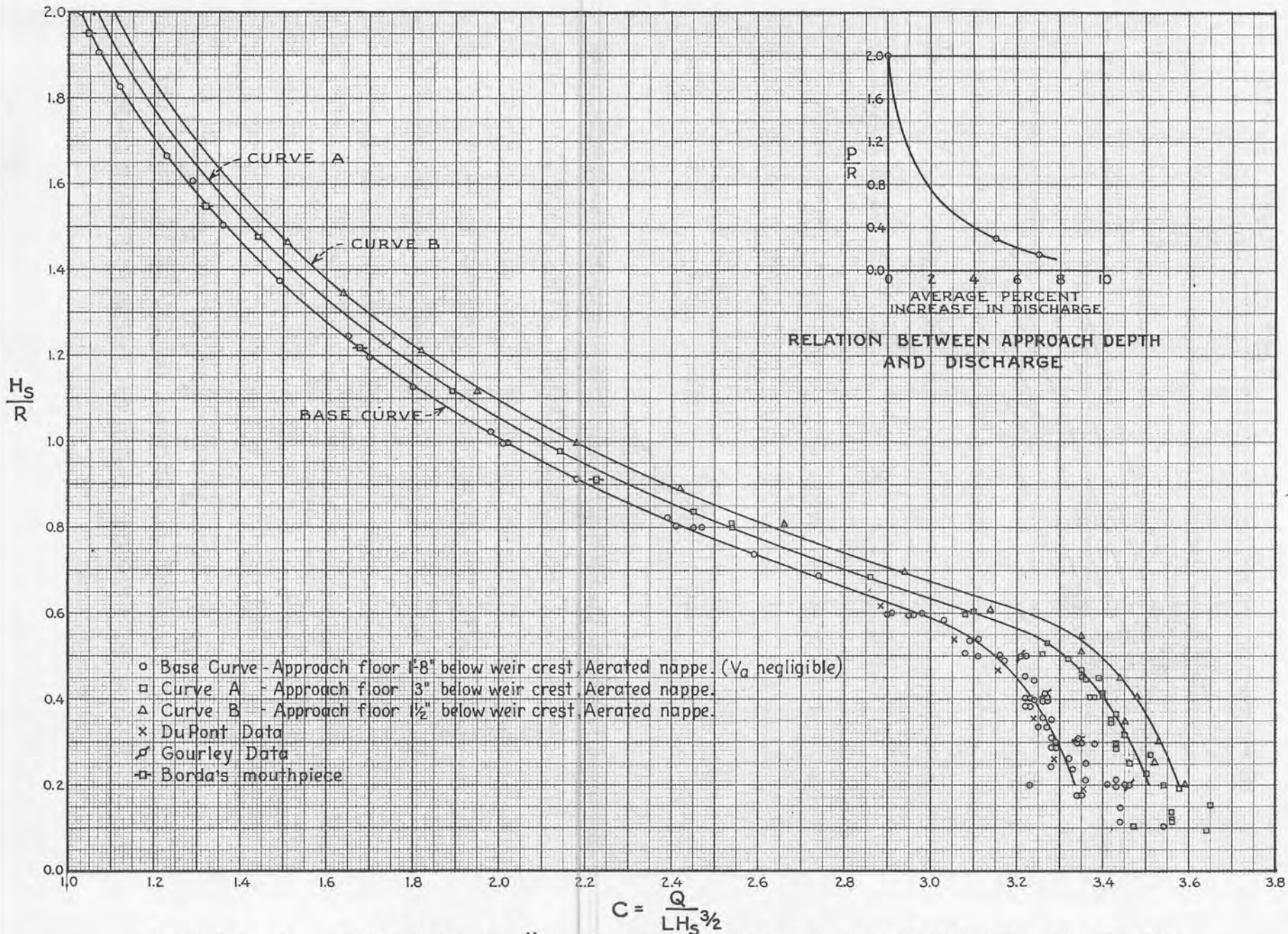

FIGURE 9. RELATION OF H_S/R TO COEFFICIENT OF DISCHARGE FOR DIFFERENT APPROACH DEPTHS (AERATED NAPPE)

FIGURE 10

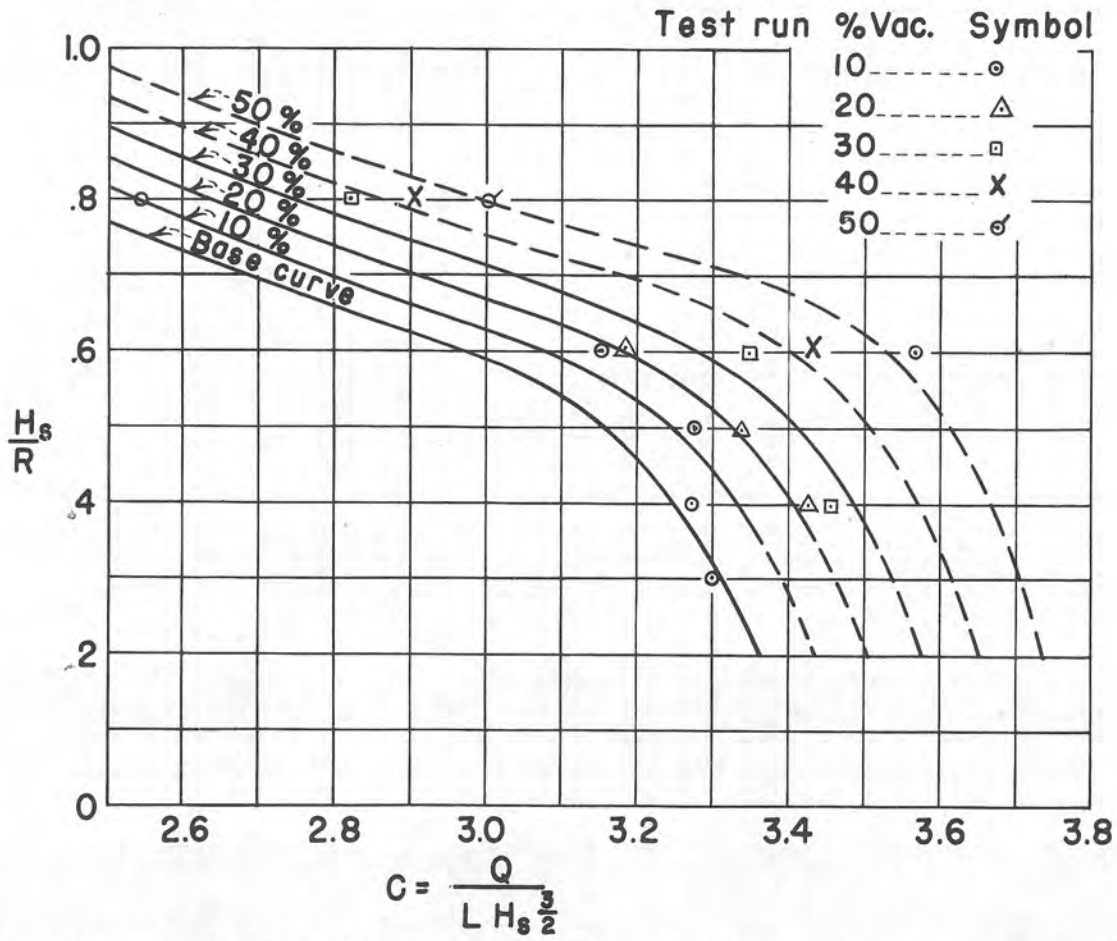

A. RELATION BETWEEN $\frac{H_s}{R}$ AND COEFFICIENT OF DISCHARGE FOR VARIOUS VACUUMS UNDER THE NAPPE

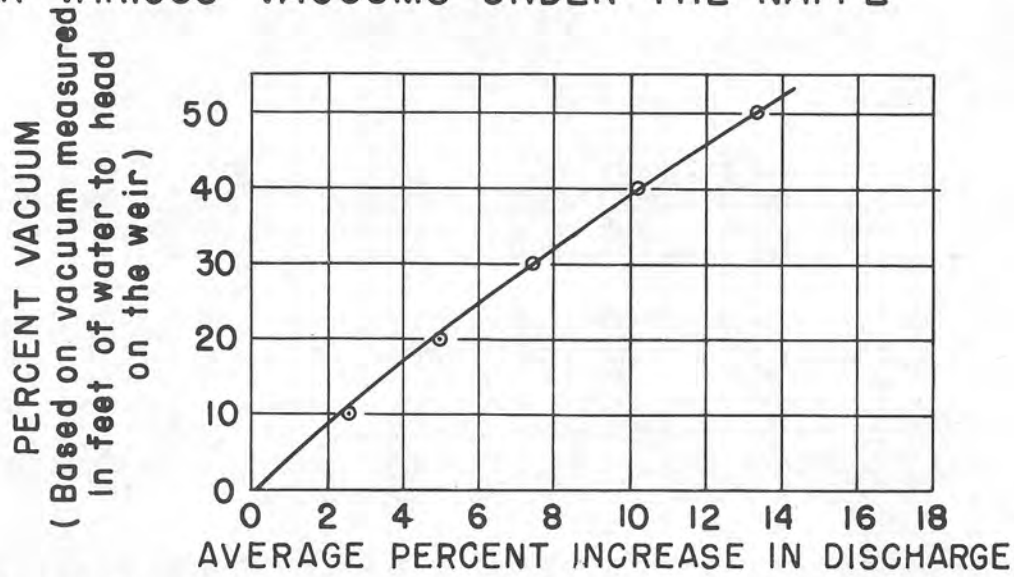

B. RELATION BETWEEN VACUUM UNDER THE NAPPE AND DISCHARGE

Referring to Figures 8 and 9, the flow apparently is free for $\frac{H_s}{R}$ ratios under 0.45. In the range of free flow, the discharge coefficient decreases almost linearly from 3.34 to 3.20 between $\frac{H_s}{R}$ ratios of 0.20 and 0.45, respectively. These coefficients compare favorably with the results obtained by other experimenters. 1/ 2/ 3/

As the $\frac{H_s}{R}$ ratio increases above 0.45, the weir becomes partially submerged and there is a sharp reduction in the coefficient of discharge. The largest change in coefficient for a relatively small rise in $\frac{H_s}{R}$ occurs for $\frac{H_s}{R}$ ratios between 0.45 and 1.00, the range in which the weir is partially submerged. For $\frac{H_s}{R}$ above 1.00, the water surface above the weir is practically level and the flow is submerged.

The two upper curves, A and B, Figure 9, are similar plots indicating the coefficient of discharge when the approach velocity is appreciable. Curve A was plotted from data obtained with the approach floor 3 inches below the weir crest, and Curve B with the approach depth 1.5 inches. The 3-inch approach depth increased the discharge coefficient approximately 5 percent over the base curve in the free-flow range of discharges and 4 percent in the range of submerged flow, while the 1.5-inch approach depth increased the coefficients approximately 7 percent and 8 percent, respectively.

In the insert of Figure 9, the average increase in discharge, in percent, is plotted versus the approach depth, P, in terms of radius of weir. This curve, which is applicable to either free or submerged flow, indicates the increase in discharge which can be expected when the approach velocity is increased (or the approach depth decreased) using the discharge for negligible velocity of approach as the base. It is evident that additional experimental data are needed in the range of $\frac{P}{R}$ ratios between 0.3 and 1.0 to fully establish the curve. However, the curve indicates the approximate increase in discharge as the approach depth decreases.

Figure 10 is a similar plot showing the relation of various pressures beneath the nappe and the discharge with negligible velocity of approach. Figure 10A shows the discharge coefficient versus $\frac{H_s}{R}$ ratios for atmospheric pressure and partial vacuums of 10, 20, 30, 40, and 50 percent under the nappe. The partial vacuums are expressed as a ratio of the average vacuum, measured in feet of water in the air chamber beneath the nappe, to the head, H_s, on the weir. The solid

lines indicate the portion of the curve verified by experimental data and the dotted lines indicate the estimated extension of the curves beyond the limits of testing in these experiments.

Figure 10B was plotted from the data contained in Figure 10A. The percent increase in discharge above that indicated by the base curve was computed for $\frac{H_s}{R}$ ratios of 0.3, 0.4, and 0.5 and 10- to 50-percent vacuums. The computed percentages for each of the five vacuums were averaged and plotted as shown in Figure 10B. This figure indicates the average increase in discharge for different pressures beneath the nappe. The relationship is applicable only in the range of free flow, since no tests with partial vacuums were made when the weir was flowing submerged. The curves presented in Figure 10 should be treated with reservation since they are based on meager experimental data.

The minimum value of $\frac{H_s}{R}$ ratio, for which discharge coefficients are shown in Figures 9 and 10, is 0.20. It was found that, for runs with heads less than 0.15 foot, the discharge coefficient was inconsistent and tended to increase as the head decreased. At low heads, surface tension of the water affects the flow characteristics by preventing the jet from springing clear at the sharp-edged crest of the weir. It is difficult to define the limits of this effect as the sharpness of the weir or a small amount of oil can change its intensity. J. W. Howe 4/ in summarizing the results of several experimenters, showed graphically that the discharge coefficient for the rectangular weir increases sharply for heads less than 0.20 foot, thus indicating the heads at which surface tension affects the discharge. Therefore, the coefficients for the test weir are shown only for heads above the region of low flow where surface tension has a marked effect.

Nappe Profiles

Figure 8 shows the general shapes of the upper and lower surface of the nappe, expressed in terms of head, with aerated nappe and negligible velocity of approach for representative $\frac{H_s}{R}$ ratios. Also included in the figure is the lower nappe shape developed by the Bureau of Reclamation 5/ for the rectangular weir, which may be considered a circular weir having an infinite radius, or $\frac{H_s}{R} = 0$.

Several attempts were made to obtain a profile for $\frac{H_s}{R} = 0.10$ (or a head of 0.083 foot on test weir), but all the measured profiles for this head were comparatively flat near the weir crest and inconsistent with the other results, indicating that the nappe adhered to the weir crest. In Table 1, the coordinates for $\frac{H_s}{R} = 0.10$ are shown, but the

profile was determined by interpolation between $\frac{H_s}{R} = 0.20$ and 0; rather than by actual nappe measurements on the test weir.

The lower nappe traces, expressed in dimensionless coordinates, in Figure 8, give a false impression as to the actual shape of the lower surface for different heads, since the coordinates in terms of the head, H_s, become progressively less as H_s increases. To illustrate the shape the profile takes as the head increases, typical lower nappe profiles, expressed in true X and Y coordinates for several $\frac{H_s}{R}$ ratios are shown for the test weir in Figure 11.

In the case of the rectangular weir, the lower nappe traces spring farther from the weir crest as the head increases. This is not true, however, with the circular weir. In Figure 11, it can be seen that, for an increase in head or $\frac{H_s}{R}$ ratio, the profile springs farther from the weir crest only in the region of the high point of the trace. Below the weir crest the traces cross and the profile for the higher head falls inside those for the lower head. Therefore, if a morning-glory spillway is designed for the maximum head, it appears that subatmospheric pressures along the lower portion of the trace will occur for heads less than maximum. To determine the extent of the subatmospheric pressures for different $\frac{H_s}{R}$ ratios was beyond the scope of these experiments. However, model tests on the morning-glory spillway for Hungry Horse Dam disclosed that any reduction in pressure for heads less than the design head could not be discerned on the model.

Hungry Horse Dam Spillway was designed for a maximum discharge of 53,000 second feet at a head of 16.9 feet with an $\frac{H_s}{R}$ ratio of approximately 0.50 and a 30-percent vacuum crest. Pressures observed on the model crest averaged approximately 5, 3, and 1.5 feet of water (prototype) below atmospheric for discharges of 50,000, 35,000, and 15,000 second feet, respectively. The observed absolute pressure, at all piezometers along the spillway crest, increased with each lower head or discharge. This example is inconclusive for the entire range of $\frac{H_s}{R}$ ratios, but it indicates that spillway crests designed for $\frac{H_s}{R}$ ratios less than 0.50 will operate at approximately atmospheric pressure for discharges lower than the maximum.

The $\frac{X}{H_s}$ and $\frac{Y}{H_s}$ coordinates of the lower nappe surface for $\frac{H_s}{R}$ ratios from 0 to 2.0, with fully aerated nappe and negligible velocity of approach are tabulated in Table 1.

The effects of velocity of approach on the lower nappe surface are shown in Figure 12, where the profiles for $\frac{P}{R}$ ratios of 2.0 (negligible approach velocity), 0.30, and 0.15 are plotted for an $\frac{H_S}{R}$ ratio of 0.40, which is typical of the profiles obtained for other $\frac{H_S}{R}$ ratios. As the approach velocity increases (or as $\frac{P}{R}$ decreases), the contraction of the jet decreases and the nappe springs less distant from the weir crest. As the water falls below the weir crest, a solid jet forms and the lower nappe profiles become similar in shape, with the profile for the higher approach velocity falling slightly inside the profile for the lower velocity of approach. Below the point where a solid jet forms, the location of the lower nappe surface is governed by the diameter of jet necessary to accommodate the discharge.

Lower nappe shapes for appreciable velocity of approach with fully aerated nappe are tabulated in Table 2.

Figure 13 shows the profiles for $\frac{H_S}{R} = 0.40$ when a partial vacuum is placed under the nappe. In general, the profiles are similar in shape, but not as flat near the crest, as those obtained with velocity of approach. As the pressure under the nappe is decreased, the profiles for a constant head fall progressively closer to the weir wall. In other words, the diameter (or area) of the jet at any point along the profile becomes progressively greater as the pressure under the nappe is decreased.

The $\frac{X}{H_S}$ and $\frac{Y}{H_S}$ coordinates of the lower nappe profile for negligible velocity of approach and partial vacuums under the nappe are tabulated in Table 3.

Upper nappe profiles in dimensionless coordinates for negligible approach velocity and aerated nappe are tabulated in Table 4. The water surface is level for $\frac{H_S}{R}$ ratios above 1.0.

The effect on the upper nappe profiles for lowered pressures beneath the nappe and increased velocity of approach was similar to that observed on the lower nappe shapes. After passing the weir crest, the upper water surface fell progressively lower for each increasing vacuum beneath the jet, and when the approach velocity was increased, a higher upper nappe surface and boil were observed.

The $\frac{X}{H_S}$ and $\frac{Y}{H_S}$ coordinates of the upper water surface are tabulated in Table 5 for aerated nappe and approach depths of $\frac{P}{R} = 0.30$

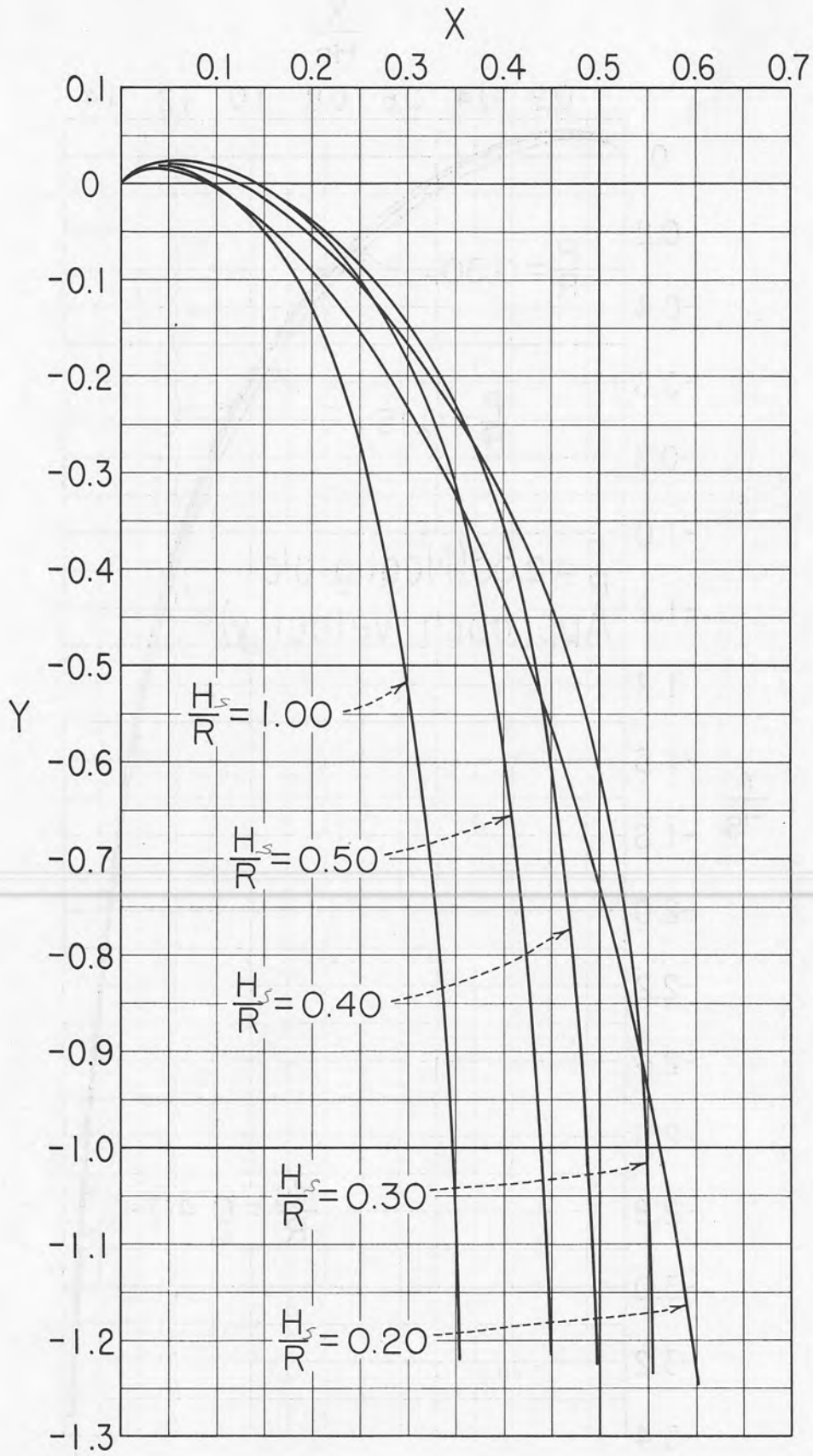

FIGURE II - TYPICAL LOWER NAPPE PROFILES IN X AND Y COORDINATES

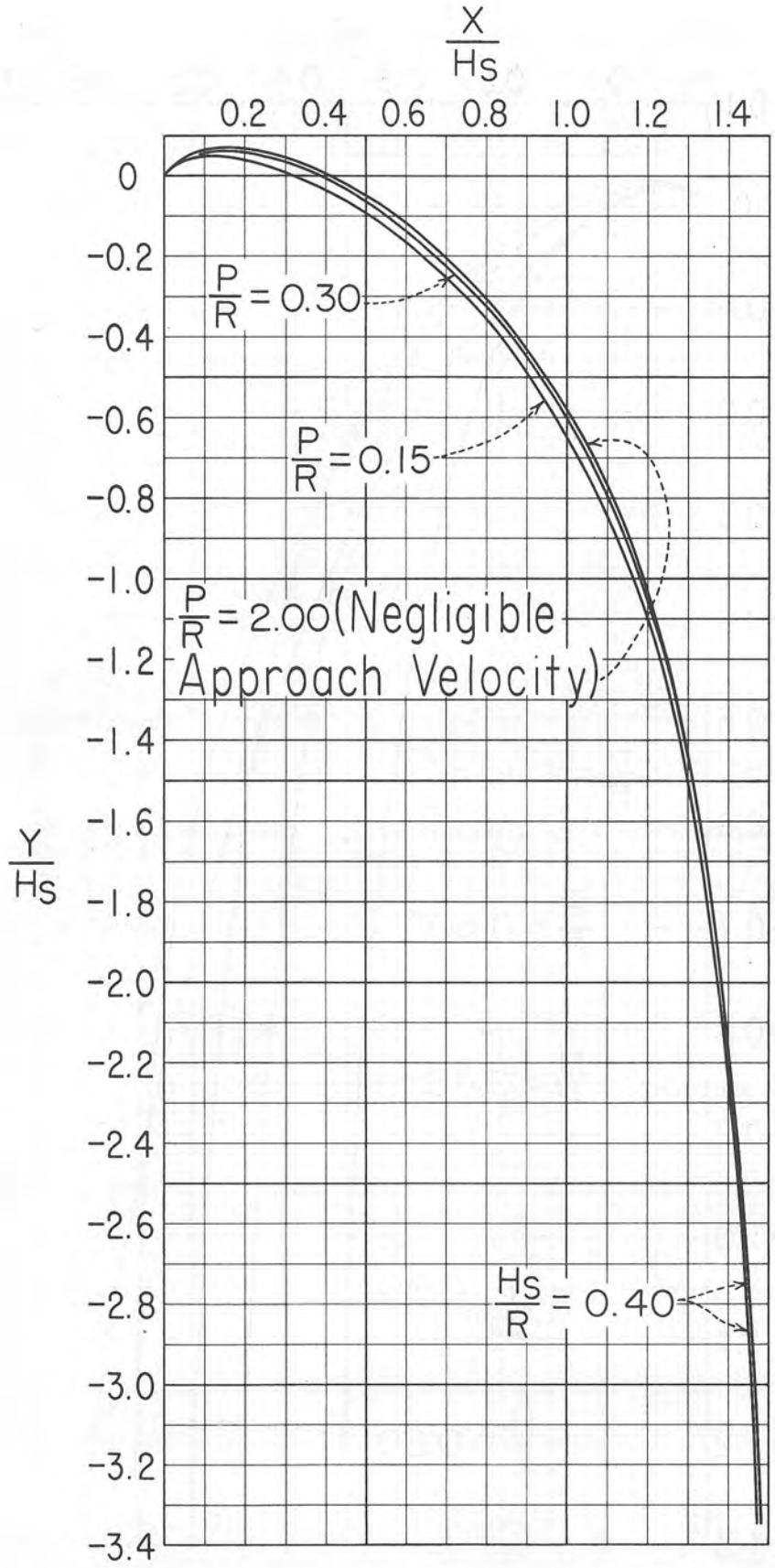

FIGURE 12- TYPICAL LOWER NAPPE PROFILE SHOWING EFFECT OF VELOCITY OF APPROACH

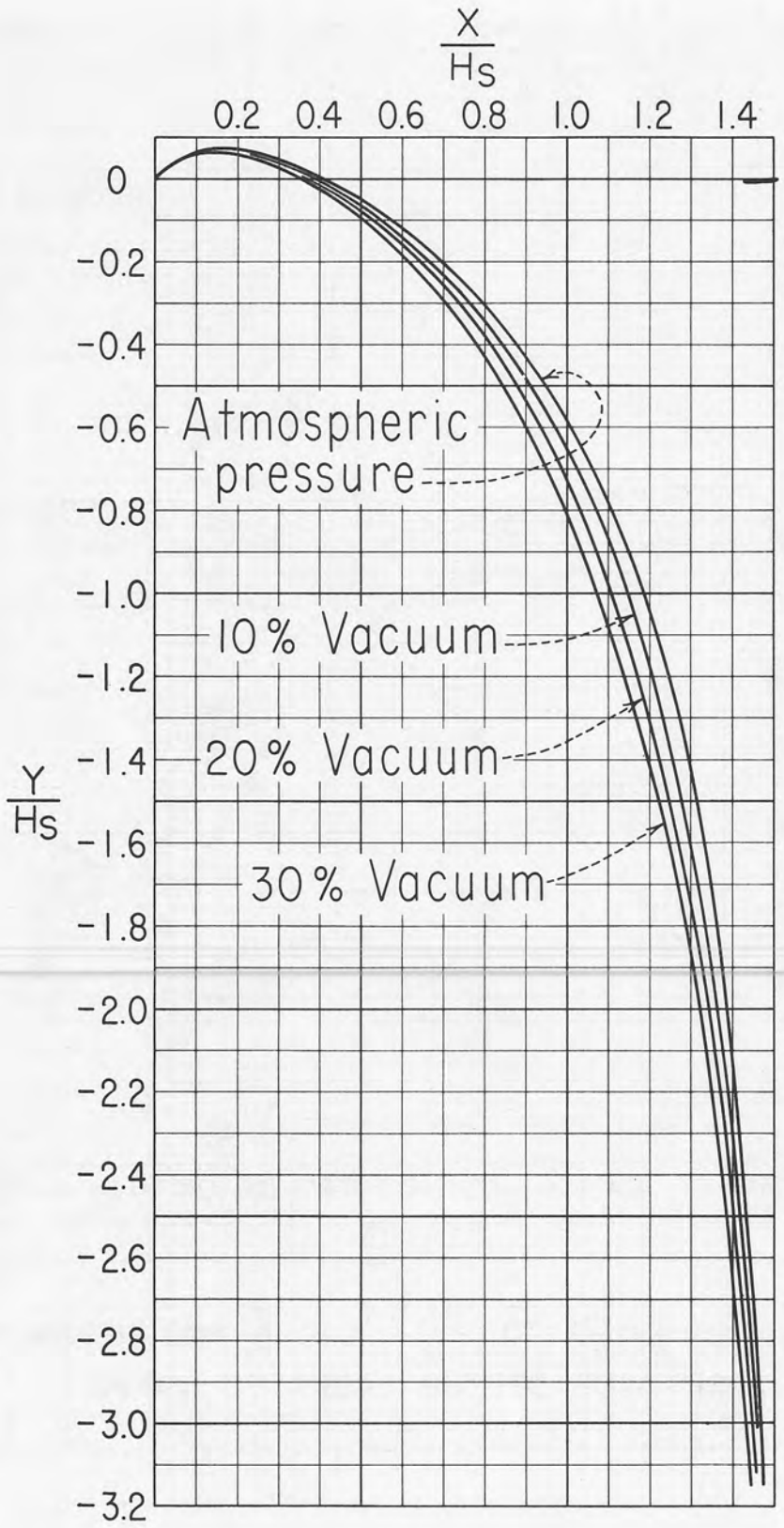

FIGURE 13- TYPICAL LOWER NAPPE PROFILE SHOWING EFFECT OF LOWERED PRESSURES UNDER THE NAPPE

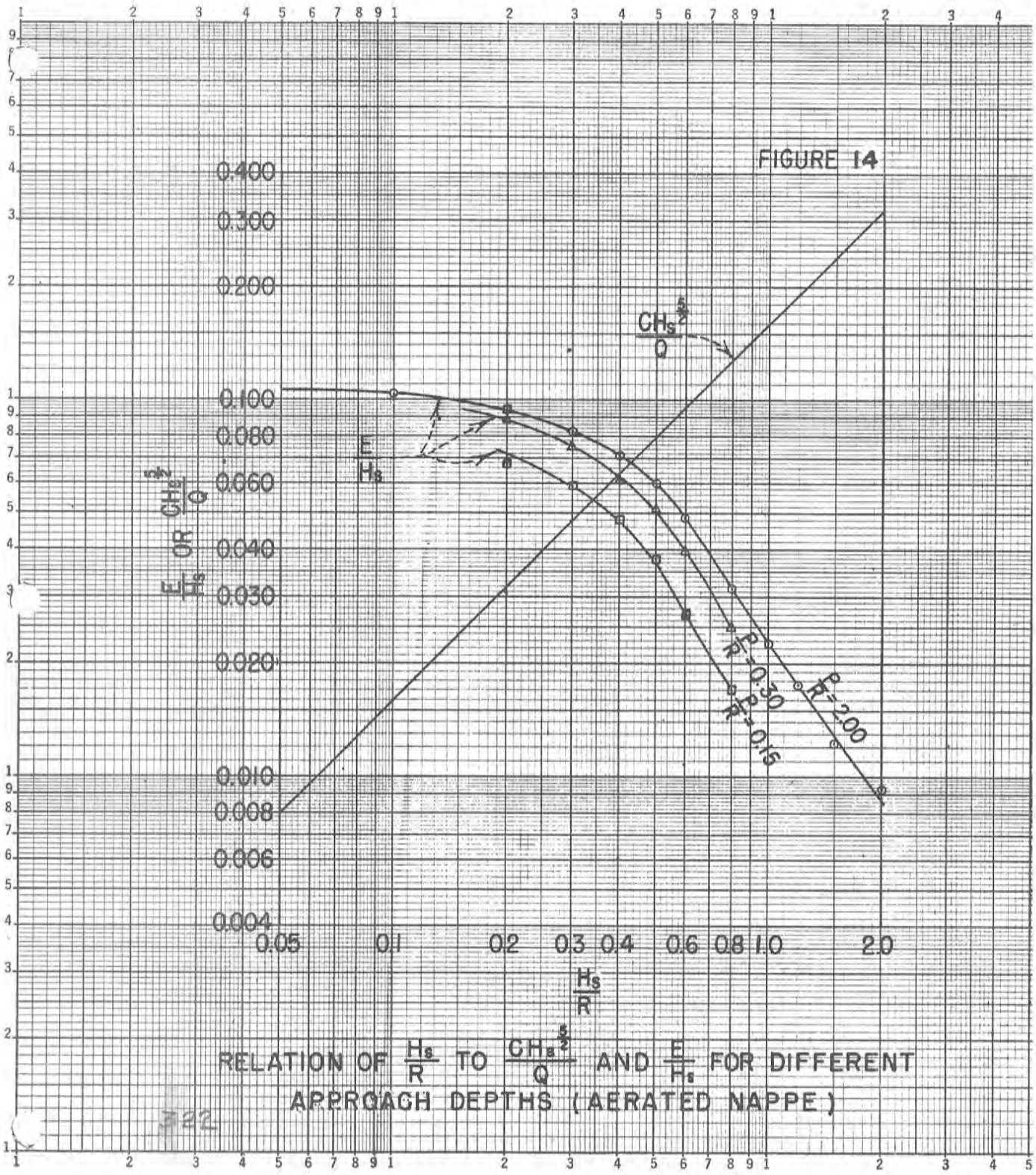

FIGURE 14

RELATION OF $\frac{H_s}{R}$ TO $\frac{CH_s^{\frac{3}{2}}}{Q}$ AND $\frac{E}{H_s}$ FOR DIFFERENT APPROACH DEPTHS (AERATED NAPPE)

FIGURE 15

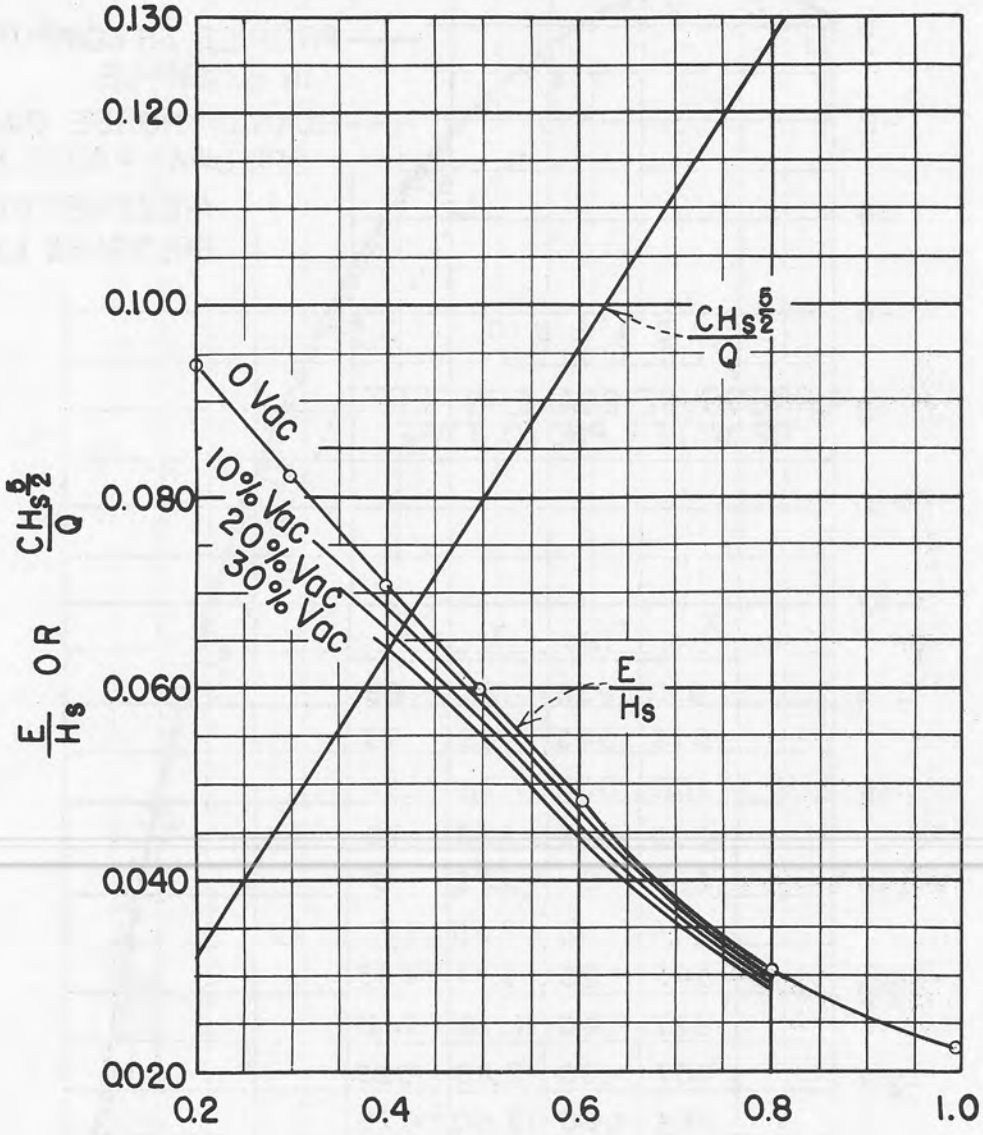

RELATION OF $\frac{H_s}{R}$ TO $\frac{CH_s^{\frac{5}{2}}}{Q}$ AND $\frac{E}{H_s}$ FOR DIFFERENT PRESSURES UNDER THE NAPPE. (NEGLIGIBLE VELOCITY OF APPROACH).

FIGURE 16

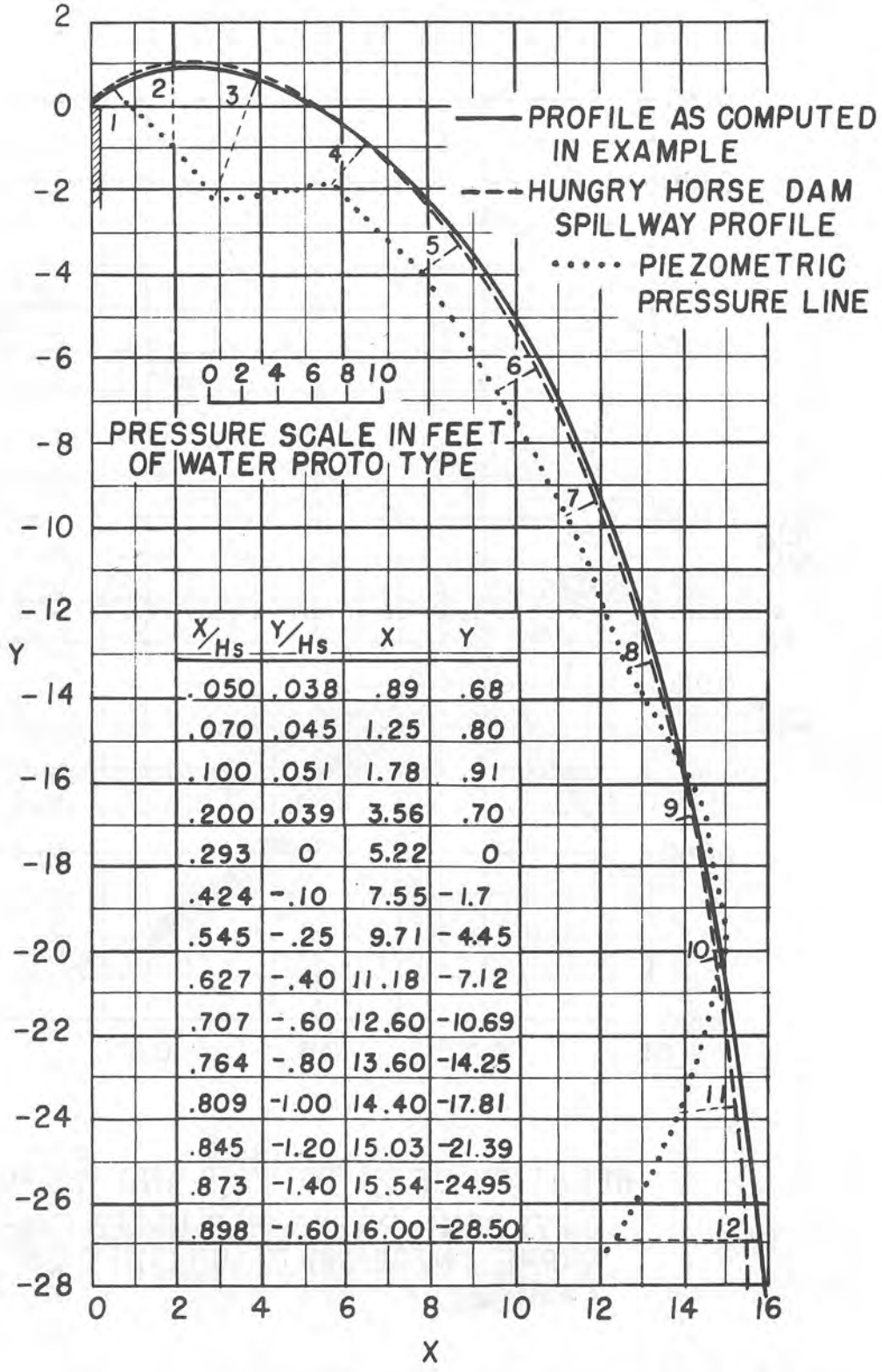

X/Hs	Y/Hs	X	Y
.050	.038	.89	.68
.070	.045	1.25	.80
.100	.051	1.78	.91
.200	.039	3.56	.70
.293	0	5.22	0
.424	-.10	7.55	-1.7
.545	-.25	9.71	-4.45
.627	-.40	11.18	-7.12
.707	-.60	12.60	-10.69
.764	-.80	13.60	-14.25
.809	-1.00	14.40	-17.81
.845	-1.20	15.03	-21.39
.873	-1.40	15.54	-24.95
.898	-1.60	16.00	-28.50

COMPARISON OF SPILLWAY PROFILES

Table 1

COORDINATES OF LOWER NAPPE SURFACE FOR DIFFERENT VALUES OF $\frac{H_s}{R}$

(Negligible approach velocity and aerated nappe)

$\frac{X}{H_s}$ \ $\frac{H_s}{R}$	0.00	*0.10	0.20	0.25	0.30	0.35	0.40	0.45	0.50	0.60	0.80	1.00	1.20	1.50	2.00
	$\frac{Y}{H_s}$														
0.000	0.0000	0.0000	0.0000	0.0000	0.0000	0.0000	0.0000	0.0000	0.0000	0.0000	0.0000	0.0000	0.0000	0.0000	0.0000
.010	.0150	.0145	.0133	.0130	.0128	.0125	.0122	.0119	.0116	.0112	.0104	.0095	.0086	.0077	.0070
.020	.0280	.0265	.0250	.0243	.0236	.0231	.0225	.0220	.0213	.0202	.0180	.0159	.0140	.0115	.0090
.030	.0395	.0365	.0350	.0337	.0327	.0317	.0308	.0299	.0289	.0270	.0231	.0198	.0168	.0126	.0085
.040	.0490	.0460	.0435	.0417	.0403	.0389	.0377	.0363	.0351	.0324	.0268	.0220	.0176	.0117	.0050
.050	.0575	.0535	.0506	.0487	.0471	.0454	.0436	.0420	.0402	.0368	.0292	.0226	.0168	.0092	
.060	.0650	.0605	.0570	.0550	.0531	.0510	.0489	.0470	.0448	.0404	.0305	.0220	.0147	.0053	
.070	.0710	.0665	.0627	.0605	.0584	.0560	.0537	.0514	.0487	.0432	.0308	.0201	.0114	.0001	
.080	.0765	.0710	.0677	.0655	.0630	.0603	.0578	.0550	.0521	.0455	.0301	.0172	.0070		
.090	.0820	.0765	.0722	.0696	.0670	.0640	.0613	.0581	.0549	.0471	.0287	.0135	.0018		
.100	.0860	.0810	.0762	.0734	.0705	.0672	.0642	.0606	.0570	.0482	.0264	.0089			
.120	.0940	.0880	.0826	.0790	.0758	.0720	.0683	.0640	.0596	.0483	.0195				
.140	.1000	.0935	.0872	.0829	.0792	.0750	.0705	.0654	.0599	.0460	.0101				
.160	.1045	.0980	.0905	.0855	.0812	.0765	.0710	.0651	.0585	.0418					
.180	.1080	.1010	.0927	.0872	.0820	.0766	.0705	.0637	.0559	.0361					
.200	.1105	.1025	.0938	.0877	.0819	.0756	.0688	.0611	.0521	.0292					
.250	.1120	.1035	.0926	.0850	.0773	.0683	.0596	.0495	.0380	.0068					
.300	.1105	.1000	.0850	.0764	.0668	.0559	.0446	.0327	.0174						
.350	.1060	.0930	.0750	.0650	.0540	.0410	.0280	.0125							
.400	.0970	.0830	.0620	.0500	.0365	.0220	.0060								
.450	.0845	.0700	.0450	.0310	.0170	.000									
.500	.0700	.0520	.0250	.0100											
.550	.0520	.0320	.0020												
.600	.0320	.0080													
.650	.0090														

Note: The above tabulation is for that portion of the profile above the weir crest.

$\frac{Y}{H_s}$ \ $\frac{H_s}{R}$	0.00	0.10	0.20	0.25	0.30	0.35	0.40	0.45	0.50	0.60	0.80	1.00	1.20	1.50	2.00
	$\frac{X}{H_s}$														
0.000	0.668	0.615	0.554	0.520	0.487	0.450	0.413	0.376	0.334	0.262	0.158	0.116	0.093	0.070	0.048
-0.020	0.705	0.652	0.592	0.560	0.526	0.488	0.452	0.414	0.369	.293	.185	.145	.120	.096	.074
-0.040	0.742	0.688	0.627	0.596	0.563	0.524	0.487	0.448	0.400	.320	.212	.165	.140	.115	.088
-0.060	0.777	0.720	0.660	0.630	0.596	0.557	0.519	0.478	0.428	.342	.232	.182	.155	.129	.100
-0.080	0.808	0.752	0.692	0.662	0.628	0.589	0.549	0.506	0.454	.363	.250	.197	.169	.140	.110
-0.100	0.838	0.784	0.722	0.692	0.657	0.618	0.577	0.532	0.478	.381	.266	.210	.180	.150	.118
-0.150	0.913	0.857	0.793	0.762	0.725	0.686	0.641	0.589	0.531	.423	.299	.238	.204	.170	.132
-0.200	0.978	0.925	0.860	0.826	0.790	0.745	0.698	0.640	0.575	.459	.326	.260	.224	.184	.144
-0.250	1.040	0.985	0.919	0.883	0.847	0.801	0.750	0.683	0.613	.490	.348	.280	.239	.196	.153
-0.300	1.100	1.043	0.976	0.941	0.900	0.852	0.797	0.722	0.648	.518	.368	.296	.251	.206	.160
-0.400	1.207	1.150	1.079	1.041	1.000	0.944	0.880	0.791	0.706	.562	.400	.322	.271	.220	.168
-0.500	1.308	1.246	1.172	1.131	1.087	1.027	0.951	0.849	0.753	.598	.427	.342	.287	.232	.173
-0.600	1.397	1.335	1.260	1.215	1.167	1.102	1.012	0.898	0.793	.627	.449	.359	.300	.240	.179
-0.800	1.563	1.500	1.422	1.369	1.312	1.231	1.112	0.974	0.854	.673	.482	.384	.320	.253	.184
-1.000	1.713	1.646	1.564	1.508	1.440	1.337	1.189	1.030	0.899	.710	.508	.402	.332	.260	.188
-1.200	1.846	1.780	1.691	1.635	1.553	1.422	1.248	1.074	0.933	.739	.528	.417	.340	.266	
-1.400	1.970	1.903	1.808	1.748	1.653	1.492	1.293	1.108	0.963	.760	.542	.423	.344		
-1.600	2.085	2.020	1.918	1.855	1.742	1.548	1.330	1.133	0.988	.780	.553	.430			
-1.800	2.196	2.130	2.024	1.957	1.821	1.591	1.358	1.158	1.008	.797	.563	.433			
-2.000	2.302	2.234	2.126	2.053	1.891	1.630	1.381	1.180	1.025	.810	.572				
-2.500	2.557	2.475	2.354	2.266	2.027	1.701	1.430	1.221	1.059	.838	.588				
-3.000	2.778	2.700	2.559	2.428	2.119	1.748	1.468	1.252	1.086	.853					
-3.500		2.916	2.749	2.541	2.171	1.777	1.489	1.267	1.102						
-4.000		3.114	2.914	2.620	2.201	1.796	1.500	1.280							
-4.500		3.306	3.053	2.682	2.220	1.806	1.509								
-5.000		3.488	3.178	2.734	2.227	1.811									
-5.500		3.653	3.294	2.779	2.229										
-6.000		3.820	3.405	2.812	2.232										

Note: The above tabulation is for that portion of the profile below the weir crest.

*The tabulation for $\frac{H_s}{R} = 0.10$ was obtained by interpolation between $\frac{H_s}{R} = 0$ and 0.20.

Table 2

COORDINATES OF LOWER NAPPE SURFACE FOR DIFFERENT VALUES OF $\frac{H_s}{R}$ AND $\frac{P}{R}$

(Aerated nappe)

$\frac{X}{H_s}$ \ $\frac{H_s}{R}$	$\frac{Y}{H_s}$ $\frac{P}{R}$ = 0.30									$\frac{P}{R}$ = 0.15								
	0.20	0.25	0.30	0.35	0.40	0.45	0.50	0.60	0.80	0.20	0.25	0.30	0.35	0.40	0.45	0.50	0.60	0.80
0.000	0.0000	0.0000	0.0000	0.0000	0.0000	0.0000	0.0000	0.0000	0.0000	0.0000	0.0000	0.0000	0.0000	0.0000	0.0000	0.0000	0.0000	0.0000
.010	.0130	.0130	.0130	.0125	.0120	.0120	.0115	.0110	.0100	.0120	.0120	.0115	.0115	.0110	.0110	.0105	.0100	.0090
.020	.0245	.0242	.0240	.0235	.0225	.0210	.0195	.0180	.0170	.0210	.0200	.0195	.0190	.0185	.0180	.0170	.0160	.0140
.030	.0340	.0335	.0330	.0320	.0300	.0290	.0270	.0240	.0210	.0285	.0270	.0265	.0260	.0250	.0235	.0225	.0200	.0165
.040	.0415	.0411	.0390	.0380	.0365	.0350	.0320	.0285	.0240	.0345	.0335	.0325	.0310	.0300	.0285	.0265	.0230	.0170
.050	.0495	.0470	.0455	.0440	.0420	.0395	.0370	.0325	.0245	.0405	.0385	.0375	.0360	.0345	.0320	.0300	.0250	.0170
.060	.0560	.0530	.0505	.0490	.0460	.0440	.0405	.0350	.0250	.0450	.0430	.0420	.0400	.0380	.0355	.0330	.0265	.0165
.070	.0610	.0575	.0550	.0530	.0500	.0470	.0440	.0370	.0245	.0495	.0470	.0455	.0430	.0410	.0380	.0350	.0270	.0150
.080	.0660	.0620	.0590	.0565	.0530	.0500	.0460	.0385	.0235	.0525	.0500	.0485	.0460	.0435	.0400	.0365	.0270	.0130
.090	.0705	.0660	.0625	.0595	.0550	.0520	.0480	.0390	.0215	.0560	.0530	.0510	.0480	.0455	.0420	.0370	.0265	.0100
.100	.0740	.0690	.0660	.0620	.0575	.0540	.0500	.0395	.0190	.0590	.0560	.0535	.0500	.0465	.0425	.0375	.0255	.0065
.120	.0800	.0750	.0705	.0650	.0600	.0560	.0510	.0380	.0120	.0630	.0600	.0570	.0520	.0480	.0435	.0365	.0220	
.140	.0840	.0790	.0735	.0670	.0615	.0560	.0515	.0355	.0020	.0660	.0620	.0585	.0525	.0475	.0425	.0345	.0175	
.160	.0870	.0810	.0750	.0675	.0610	.0550	.0500	.0310		.0670	.0635	.0590	.0520	.0460	.0400	.0305	.0110	
.180	.0885	.0820	.0755	.0675	.0600	.0535	.0475	.0250		.0675	.0635	.0580	.0500	.0435	.0365	.0260	.0040	
.200	.0885	.0820	.0745	.0660	.0575	.0505	.0435	.0180		.0670	.0625	.0560	.0465	.0395	.0320	.0200		
.250	.0855	.0765	.0685	.0590	.0480	.0390	.0270			.0615	.0560	.0470	.0360	.0265	.0160	.0015		
.300	.0780	.0670	.0580	.0460	.0340	.0220	.0050			.0520	.0440	.0330	.0210	.0100				
.350	.0660	.0540	.0425	.0295	.0150					.0380	.0285	.0165	.0030					
.400	.0495	.0370	.0240	.0100						.0210	.0090							
.450	.0300	.0170	.0025							.0015								
.500	.0090	-.0060																
.550																		

Note: The above tabulation is for that portion of the profile above the crest.

$\frac{Y}{H_s}$ \ $\frac{H_s}{R}$	$\frac{X}{H_s}$								
	0.20	0.25	0.30	0.35	0.40	0.45	0.50	0.60	0.80
-0.000	0.519	0.488	0.455	0.422	0.384	0.349	0.310	0.238	0.144
-0.020	0.560	0.528	0.495	0.462	0.423	0.387	0.345	.272	.174
-0.040	0.598	0.566	0.532	0.498	0.458	0.420	0.376	.300	.198
-0.060	0.632	0.601	0.567	0.532	0.491	0.451	0.406	.324	.220
-0.080	0.664	0.634	0.600	0.564	0.522	0.480	0.432	.348	.238
-0.100	0.693	0.664	0.631	0.594	0.552	0.508	0.456	.368	.254
-0.150	0.760	0.734	0.701	0.661	0.618	0.569	0.510	.412	.290
-0.200	0.831	0.799	0.763	0.723	0.677	0.622	0.558	.451	.317
-0.250	0.893	0.860	0.826	0.781	0.729	0.667	0.599	.483	.341
-0.300	0.953	0.918	0.880	0.832	0.779	0.708	0.634	.510	.362
-0.400	1.060	1.024	0.981	0.932	0.867	0.780	0.692	.556	.396
-0.500	1.156	1.119	1.072	1.020	0.938	0.841	0.745	.595	.424
-0.600	1.242	1.203	1.153	1.098	1.000	0.891	0.780	.627	.446
-0.800	1.403	1.359	1.301	1.227	1.101	0.970	0.845	.672	.478
-1.000	1.549	1.498	1.430	1.333	1.180	1.028	0.892	.707	.504
-1.200	1.680	1.622	1.543	1.419	1.240	1.070	0.930	.733	.524
-1.400	1.800	1.739	1.647	1.489	1.287	1.106	0.959	.757	.540
-1.600	1.912	1.849	1.740	1.546	1.323	1.131	0.983	.778	.551
-1.800	2.018	1.951	1.821	1.590	1.353	1.155	1.005	.797	.560
-2.000	2.120	2.049	1.892	1.627	1.380	1.175	1.022	.810	.569
-2.500	2.351	2.261	2.027	1.697	1.428	1.218	1.059	.837	
-3.000	2.557	2.423	2.113	1.747	1.464	1.247	1.081	.852	
-3.500	2.748	2.536	2.167	1.778	1.489	1.263	1.099		
-4.000	2.911	2.617	2.200	1.796	1.499	1.274			
-4.500	3.052	2.677	2.217	1.805	1.507				
-5.000	3.173	2.731	2.223	1.810					
-5.500	3.290	2.773	2.228						
-6.000	3.400	2.808							

$\frac{X}{H_s}$	$\frac{P}{R}$ = 0.15								
	0.20	0.25	0.30	0.35	0.40	0.45	0.50	0.60	0.80
	0.454	0.422	0.392	0.358	0.325	0.288	0.253	0.189	0.116
	0.499	0.467	0.437	0.404	0.369	0.330	0.292	.228	.149
	0.540	0.509	0.478	0.444	0.407	0.368	0.328	.259	.174
	0.579	0.547	0.516	0.482	0.443	0.402	0.358	.286	.195
	0.615	0.583	0.550	0.516	0.476	0.434	0.386	.310	.213
	0.650	0.616	0.584	0.547	0.506	0.462	0.412	.331	.228
	0.726	0.691	0.660	0.620	0.577	0.526	0.468	.376	.263
	0.795	0.760	0.729	0.685	0.639	0.580	0.516	.413	.293
	0.862	0.827	0.790	0.743	0.692	0.627	0.557	.445	.319
	0.922	0.883	0.843	0.797	0.741	0.671	0.594	.474	.342
	1.029	0.988	0.947	0.893	0.828	0.749	0.656	.523	.381
	1.128	1.086	1.040	0.980	0.902	0.816	0.710	.567	.413
	1.220	1.177	1.129	1.061	0.967	0.869	0.753	.601	.439
	1.380	1.337	1.285	1.202	1.080	0.953	0.827	.655	.473
	1.525	1.481	1.420	1.317	1.164	1.014	0.878	.696	.498
	1.659	1.610	1.537	1.411	1.228	1.059	0.917	.725	.517
	1.780	1.731	1.639	1.480	1.276	1.096	0.949	.750	.531
	1.897	1.843	1.729	1.533	1.316	1.123	0.973	.770	.544
	2.003	1.947	1.809	1.580	1.347	1.147	0.997	.787	.553
	2.104	2.042	1.879	1.619	1.372	1.167	1.013	.801	.560
	2.340	2.251	2.017	1.690	1.423	1.210	1.049	.827	
	2.550	2.414	2.105	1.738	1.457	1.240	1.073	.840	
	2.740	2.530	2.153	1.768	1.475	1.252	1.088		
	2.904	2.609	2.180	1.780	1.487	1.263			
	3.048	2.671	2.198	1.790	1.491				
	3.169	2.727	2.207	1.793					
	3.286	2.769	2.210						
	3.396	2.800							

Note: The above tabulation is for that portion of the profile below the crest.

Table 3

COORDINATES OF LOWER NAPPE SURFACE FOR DIFFERENT VALUES OF $\frac{H_s}{R}$ AND VACUUMS

(Negligible approach velocity)

$\frac{X}{H_s}$ \ $\frac{H_s}{R}$	$\frac{Y}{H_s}$ 10-percent vacuum* 0.30	0.40	0.50	0.60	0.80	20-percent vacuum* 0.40	0.50	0.60	0.80	30-percent vacuum* 0.40	0.50	0.60	0.80
0.000	0.0000	0.0000	0.0000	0.0000	0.0000	0.0000	0.0000	0.0000	0.0000	0.0000	0.0000	0.0000	0.0000
.010	.0135	.0135	.0130	.0130	.0112	.0132	.0130	.0128	.0110	.0130	.0127	.0125	.0107
.020	.0235	.0230	.0225	.0215	.0180	.0227	.0220	.0210	.0175	.0225	.0215	.0205	.0170
.030	.0325	.0310	.0295	.0285	.0230	.0300	.0290	.0280	.0225	.0295	.0280	.0275	.0220
.040	.0395	.0375	.0350	.0330	.0265	.0370	.0340	.0325	.0260	.0365	.0335	.0320	.0250
.050	.0460	.0435	.0400	.0370	.0285	.0430	.0395	.0365	.0280	.0420	.0390	.0360	.0275
.060	.0515	.0480	.0450	.0405	.0295	.0475	.0440	.0400	.0290	.0465	.0435	.0395	.0285
.070	.0560	.0520	.0480	.0430	.0300	.0510	.0470	.0425	.0295	.0505	.0465	.0420	.0285
.080	.0600	.0565	.0520	.0450	.0295	.0555	.0505	.0445	.0290	.0540	.0495	.0440	.0280
.090	.0635	.0590	.0540	.0460	.0280	.0580	.0530	.0450	.0270	.0565	.0520	.0445	.0260
.100	.0665	.0620	.0560	.0470	.0260	.0605	.0540	.0460	.0250	.0585	.0530	.0460	.0240
.120	.0705	.0655	.0580	.0475	.0190	.0640	.0565	.0460	.0180	.0620	.0545	.0450	.0175
.140	.0730	.0680	.0580	.0450	.0105	.0660	.0565	.0435	.0095	.0630	.0545	.0420	.0090
.160	.0740	.0680	.0570	.0410	-.0010	.0660	.0550	.0395	-.0020	.0630	.0530	.0380	-.0030
.180	.0740	.0670	.0540	.0360		.0640	.0520	.0340		.0610	.0500	.0320	
.200	.0730	.0650	.0500	.0290		.0620	.0480	.0260		.0580	.0450	.0245	
.250	.0670	.0550	.0360	.0040		.0500	.0320	.0020		.0455	.0290	-.0010	
.300	.0560	.0390	.0145			.0330	.0100			.0265	.0070		
.350	.0400	.0200	-.0125			.0120	-.0180			.0030	-.0225		
.400	.0200	-.0040				-.0140				-.0240			
.450	-.0045												

Note: The above tabulation is for that portion of the profile above the weir crest.

$\frac{Y}{H_s}$ \ $\frac{H_s}{R}$	$\frac{X}{H_s}$ 0.30	0.40	0.50	0.60	0.80	0.40	0.50	0.60	0.80	0.40	0.50	0.60	0.80
0.000	0.442	0.393	0.328	0.257	0.158	0.374	0.319	0.253	0.157	0.356	0.313	0.248	0.155
-0.020	0.478	0.431	0.362	.288	.187	0.411	0.353	.284	.185	0.392	0.346	.279	.183
-0.040	0.512	0.465	0.392	.314	.210	0.444	0.383	.310	.208	0.425	0.375	.305	.205
-0.060	0.452	0.496	0.418	.338	.229	0.475	0.410	.333	.227	0.454	0.402	.328	.224
-0.080	0.572	0.525	0.444	.358	.247	0.504	0.434	.354	.244	0.482	0.426	.348	.240
-0.100	0.600	0.552	0.467	.377	.262	0.531	0.458	.372	.259	0.509	0.449	.367	.255
-0.150	0.663	0.613	0.519	.418	.295	0.592	0.508	.414	.291	0.567	0.498	.409	.287
-0.200	0.720	0.669	0.563	.454	.321	0.645	0.552	.449	.316	0.618	0.540	.443	.312
-0.250	0.773	0.718	0.601	.484	.343	0.692	0.589	.479	.339	0.664	0.577	.472	.333
-0.300	0.823	0.764	0.634	.511	.363	0.734	0.622	.506	.358	0.705	0.609	.498	.351
-0.400	0.913	0.843	0.690	.556	.395	0.813	0.678	.550	.389	0.779	0.664	.542	.381
-0.500	0.996	0.913	0.737	.593	.422	0.879	0.723	.587	.414	0.844	0.709	.578	.407
-0.600	1.068	0.973	0.779	.623	.442	0.938	0.763	.617	.435	0.900	0.749	.609	.427
-0.800	1.193	1.070	0.843	.670	.476	1.032	0.826	.663	.469	0.993	0.810	.656	.459
-1.000	1.303	1.144	0.889	.705	.501	1.108	0.873	.696	.493	1.071	0.860	.690	.483
-1.200	1.401	1.203	0.927	.732	.518	1.170	0.912	.723	.510	1.137	0.900	.716	.501
-1.400	1.492	1.253	0.955	.755	.533	1.223	0.943	.746	.525	1.193	0.931	.739	.516
-1.600	1.574	1.297	0.980	.773	.545	1.268	0.970	.765	.535	1.243	0.958	.757	.528
-1.800	1.649	1.331	1.000	.790	.555	1.307	0.991	.780	.546	1.287	0.980	.773	.538
-2.000	1.717	1.361	1.018	.803	.564	1.340	1.010	.795	.555	1.321	1.000	.785	.546
-2.500	1.865	1.420	1.053	.828	.579	1.408	1.046	.819	.571	1.389	1.039	.810	.564
-3.000	1.988	1.457	1.078	.848		1.450	1.070	.838		1.435	1.062	.830	
-3.500	2.088	1.482	1.093			1.473	1.083			1.467	1.077		
-4.000	2.158	1.498				1.490				1.483			
-4.500	2.205	1.508				1.500				1.492			
-5.000	2.228												
-5.500	2.230												
-6.000	2.231												

Note: The above tabulation is for that portion of the profile below the weir crest.

*The percentages are based on the ratio of the vacuum, measured in feet of water, to the total head on the weir.

Table 4

COORDINATES OF UPPER NAPPE SURFACE FOR DIFFERENT VALUES OF $\frac{H_s}{R}$
(Negligible Velocity of Approach and Aerated Nappe)

	$\frac{Y}{H_s}$										
$\frac{X}{H_s}$ \ $\frac{H_s}{R}$	0.20	0.25	0.30	0.35	0.40	0.45	0.50	0.60	0.80	1.00	Level water surface for $\frac{H_s}{R} > 1.00$
-0.40	0.955	0.956	0.959	0.960	0.961	0.963	0.968	0.976	0.986	1.000	
-0.20	0.925	0.927	0.929	.930	.935	.936	.942	.958	.973	0.996	
0.00	0.880	0.886	0.892	.895	.900	.905	.920	.932	.955		
0.20	0.820	0.829	0.838	.845	.851	.861	.870	.900			
0.40	0.740	0.753	0.763	.772	.787	.801	.815	.855			
0.60	0.640	0.658	0.669	.684	.702	.726	.748				
0.80	0.518	0.540	0.556	.578	.600	.633					
1.00	0.372	0.402	0.420	.449	.475						
1.20	0.205	0.240	0.265	.300	.328						
1.40	0.013	0.051	0.081	.128							
1.60	-0.205	-0.160	-0.122	-.063							
1.80	-0.457	-0.400	-0.357								
2.00	-0.748	-0.678	-0.613								
2.20	-1.072	-0.981	-0.895								
2.40	-1.440	-1.315	-1.198								
2.60	-1.845	-1.670									
2.80	-2.268										
3.00	-2.685										
Point at which upper nappe surface joins boil											
X/H_s			2.410	1.711	1.208	0.810	0.725	0.510	0.120	-0.068	
Y/H_s			-1.210	-0.185	0.320	0.626	0.696	0.825	0.940	0.990	
High point of boil											
X/H_s				2.911	2.545	2.267	2.043	1.710	1.275	1.030	
Y/H_s				0.006	0.438	0.666	0.783	0.942	0.970	1.000	

Table 5

COORDINATES OF UPPER NAPPE SURFACE FOR DIFFERENT VALUES OF $\frac{H_s}{R}$ AND $\frac{P}{R}$

(Aerated nappe)

	$\frac{Y}{H_s}$																	
	$\frac{P}{R}$ = 0.30									$\frac{P}{R}$ = 0.15								
$\frac{X}{H_s}$ \ $\frac{H_s}{R}$	0.20	0.25	0.30	0.35	0.40	0.45	0.50	0.60	0.80	0.20	0.25	0.30	0.35	0.40	0.45	0.50	0.60	0.80
-0.40	0.964	0.965	0.968	0.975	0.976	0.977	0.978	0.986	0.991	0.957	0.962	0.968	0.971	0.978	0.980	0.987	0.990	0.995
-0.20	0.929	0.934	0.936	.947	.949	.950	.954	.966	.981	0.917	0.924	.934	.942	.949	.955	.960	.970	.985
0.00	0.879	0.885	0.890	.901	.907	.911	.919	.938	.966	0.870	0.875	.887	.899	.909	.915	.922	.937	.970
0.20	0.813	0.818	0.829	.843	.853	.862	.871	.892	.944	0.800	0.810	.823	.836	.850	.860	.871	.894	.948
0.40	0.730	0.737	0.753	.772	.788	.798	.810	.836		0.715	0.727	.745	.759	.776	.792	.807	.841	
0.60	0.626	0.641	0.658	.683	.700	.715	.730			0.610	0.629	.648	.666	.686	.708	.735		
0.80	0.506	0.524	0.544	.574	.592	.611				0.490	0.511	.533	.556	.582	.612			
1.00	0.363	0.388	0.413	.442	.465					0.352	0.377	.398	.427	.465				
1.20	0.199	0.228	0.253	.292						0.187	0.216	.240	.277	.337				
1.40	0.005	0.042	0.071	.123						-0.007	0.028	.055	.106					
1.60	-0.223	-0.175	-0.135	-.070						-0.235	-0.190	-.155	-.081					
1.80	-0.482	-0.422	-0.368							-0.498	-0.437	-.388						
2.00	-0.772	-0.702	-0.625							-0.795	-0.710	-.648						
2.20	-1.083	-1.018	-0.910							-1.118	-1.023	-.903						
2.40	-1.415	-1.347	-1.235							-1.448	-1.350							
2.60	-1.767	-1.683								-1.800	-1.683							
2.80	-2.130	-2.018								-2.148	-2.035							
3.00	-2.500	-2.351								-2.522	-2.388							
Point at which upper nappe surface joins boil																		
X/H_s			2.410	1.733	1.096	0.938	0.714	0.420	0.315			2.222	1.723	1.260	0.948	0.732	0.420	0.344
Y/H_s			-1.253	-0.210	0.394	0.531	0.680	0.830	0.926			-0.932	-0.200	0.295	0.530	0.681	0.835	0.925
High point of boil																		
X/H_s			3.370	2.922	2.436	2.288		1.775	1.252				2.935	2.531	2.278	2.009	1.680	1.263
Y/H_s			-0.755	0.043	0.496	0.713		0.950	0.985				0.002	0.458	0.647	0.815	0.935	0.998

Table 6

COORDINATES OF UPPER NAPPE SURFACE FOR DIFFERENT $\frac{H_s}{R}$ RATIOS AND VACUUMS

(Negligible velocity of approach)

$\frac{Y}{H_s}$													
	10-percent vacuum*					20-percent vacuum*				30-percent vacuum*			
$\frac{X}{H_s}$ \ $\frac{H_s}{R}$	0.30	0.40	0.50	0.60	0.80	0.40	0.50	0.60	0.80	0.40	0.50	0.60	0.80
-0.40	0.940	0.951	0.956	0.963	0.981	0.941	0.950	0.958	0.978	0.939	0.945	0.957	0.975
-0.20	.911	.927	.938	.940	.971	.911	.925	.931	.966	.908	.912	.929	.964
0.00	.865	.883	.897	.909	.960	.865	.886	.898	.957	.865	.870	.890	.952
0.20	.803	.825	.848	.873	.950	.808	.835	.860	.941	.803	.815	.843	
0.40	.725	.753	.783	.825		.735	.770	.808		.723	.742	.789	
0.60	.628	.662	.711			.641	.697			.622	.650	.724	
0.80	.508	.551				.522				.491			
1.00	.358	.413				.368				.325			
1.20	.170	.242				.173				.105			
1.40	-.062	-.053				-.070				-.163			
1.60	-.327					-.345				-.460			
1.80	-.629					-.638				-.783			
2.00	-.975												
2.20	-1.374												
2.40	-1.819												
2.60	-2.300												
Point at which upper nappe surface joins boil													
X/H_s	2.600	1.504	.721	.403	.300	1.808	.722	.418	.299	1.803	.735	.608	.152
Y/H_s	-2.300	-.043	.665	.821	.944	-.644	.647	.803	.931	-.790	.620	.722	.940

*The percentages are based on the ratio of the vacuum, measured in feet of water, to the total head on the weir.

and 0.15, while in Table 6 is recorded similar upper nappe shapes with negligible approach velocity for 10, 20, and 30 percent vacuums beneath the nappe.

Relation of E and Q to Radius of Weir

In these experiments, the discharge over the sharp-crested weir was computed in terms of H_S, the total head on the test weir. In designing the overflow section of a morning-glory spillway, it is usually more convenient to begin the computations with H_O, the total head above the spillway crest. To facilitate the interchange between H_S and H_O, the relation of $\frac{H_S}{R}$ to $\frac{E}{H_S}$ for the three approach depths and the three vacuum crests is plotted in Figures 14 and 15, respectively. The values of $\frac{E}{H_S}$, which are equal to $\frac{Y}{H_S}$ at the high point of the lower nappe profile, were obtained from Tables 1, 2, and 3. Since $H_S = H_O + E$ (see Figure 1), the curves offer a means of determining H_O when H_S is known or vice versa.

Since the discharge equation for the circular weir, $Q = CLH_S^{3/2}$, involves three variables (C, L or radius, and H_S), the procedure for determining the size of the overflow section for a morning-glory spillway is by successive approximations, a long and tedious process. By expressing the discharge in terms of the dimensionless ratio $\frac{H_S}{R}$, the number of variables is reduced to two and the amount of work is minimized.

Let

$$Q = CLH_S^{3/2}$$

$$= C(2\pi R)H_S^{3/2}$$

$$= \frac{C2\pi}{\frac{H_S}{R}} H_S^{5/2}$$

Then

$$\frac{H_S}{R} = 2\pi \left(C \frac{H_S^{5/2}}{Q}\right)$$

Values of $C \frac{H_S^{5/2}}{Q}$ for different $\frac{H_S}{R}$ ratios are plotted in Figures 14 and 15. When used in conjunction with the ratio $\frac{E}{H_S}$, the number of successive approximations required to determine C, R, or H_S is materially reduced.

APPLICATION OF RESULTS

To illustrate the practical use of these experimental results in determining the profile of a morning-glory spillway, a comparison with the model studies made on Hungry Horse Dam Spillway will be shown (see page 9). Although the crest profile for Hungry Horse Dam Spillway was determined from specific tests on the circular test weir, none of the Hungry Horse data was used in these experiments.

The first step in the computations is to determine the radius of the spring point, R, required to pass 53,000 second feet when the head, H_o, above the high point of the crest is 16.9 feet. Since the experimental data are in terms of head above the weir, H_s, it is necessary to assume a value of H_s as well as a coefficient, C.

Assume $H_s = 18$ feet and $C = 3.30$

Then

$$\frac{CH_s^{5/2}}{Q} = \frac{3.30\ (18)^{5/2}}{53,000} = 0.086$$

Entering Figure 15 with this value, $\frac{H_s}{R} = 0.54$ and $\frac{E}{H_s} = 0.051$ for a 30-percent vacuum crest. Then $E = 0.051\ (18) = 0.92$ foot, and $H_s = H_o + E = 16.9 + 0.92 = 17.82$ feet. From Figure 10, find $C = 3.37$, which does not check the assumed value.

Using these new values of C and H_s, the process is repeated.

$$\frac{CH_s^{5/2}}{Q} = \frac{3.37\ (17.8)^{5/2}}{53,000} = 0.085$$

From Figure 15, $\frac{H_s}{R} = 0.53$ and $\frac{E}{H_s} = 0.051$. Therefore, $E = 0.91$ and $H_s = 17.81$ feet. From Figure 10, $C = 3.38$, which checks sufficiently close to the trial values.

Then

$$R = \frac{17.81}{0.53} = 33.6 \text{ feet}$$

The radius, R, and the head, H_s, above the weir have now been established.

With the ratio, $\frac{H_S}{R} = 0.53$, it is possible to determine the shape of the overflow section. The $\frac{X}{H_S}$ and $\frac{Y}{H_S}$ coordinates for a 30-percent vacuum crest are given for $\frac{H_S}{R}$ values of 0.50 and 0.60 in Table 3. By interpolation, sufficient coordinates to describe the curve for $\frac{H_S}{R} = 0.53$ are obtained. These $\frac{X}{H_S}$ and $\frac{Y}{H_S}$ coordinates and the corresponding X and Y values are tabulated in Figure 16. The overflow section of the spillway can now be plotted as shown in the same figure.

The following table shows a comparison of the above results with the model studies of Hungry Horse Dam Spillway.

	Experimental data	Hungry Horse Dam Spillway as designed	Hungry Horse model study results
H_S	17.81'	17.9'	17.9'
H_O	16.90'	16.9'	16.90'
E	0.91'	1.00'	1.00'
R	33.6'	34.0'	34.0'
Q	53,000 cfs	53,000 cfs	49,000 cfs
C	3.38	3.28	3.06
Vacuum crest	-5.3'	-5.0'	0.8 to -8.0'
Crest shape		see Figure 16	

Column 1 shows the significant data from these experiments used in computing the example and Column 2 lists similar terms used in the design of Hungry Horse Dam Spillway. It is noted that the experimental data show slightly lower H_S, E, and R values than those used in the Hungry Horse design, which accounts for the higher coefficient of discharge, C, obtained with the experimental data.

Since the model was constructed using the spillway dimensions listed in Column 2, the values of H_S, H_O, E, and R are identical in Columns 2 and 3. The discharge obtained in the model is approximately 7 percent less than the design flow. This discrepancy can be explained as follows: (1) The spillway is designed with a 9-foot-wide pier, placed over the rounded crest. In computing the discharge in Columns 1 and 2, the reduced effective length of the crest, due to the pier, was not considered which accounts for approximately one-half the 7-percent discrepancy. (2) The experimental data are based on the ideal situation where all the flow enters the spillway on radial lines. For Hungry Horse Dam Spillway approximately one-half of the crest is located in an approach channel cut in the hillside, and only 50 to 60 percent of the flow approaches the crest on radial lines.

Whether the reduction in discharge, due to the nonradial approach conditions, is greater or less than that indicated by the difference in the computed and model discharge cannot be determined from the available data.

A comparison of the two rounded crests is shown in Figure 16 where the profile, as determined from these experiments, is plotted as a solid line and the Hungry Horse crest is denoted by a broken line. Also shown are the piezometric pressures in feet of water (prototype) observed on the model for a discharge corresponding to a prototype flow of 50,000 second feet. Pressures above atmospheric are indicated above and to the right of the profile and subatmospheric pressures are shown below and to the left of the profile.

The greatest deviation in the two profiles occurs in the region between Piezometers 4 and 7 and at the lower end of the rounded crest between Piezometers 11 and 12. The observed pressures on the model crest suggest the true shape of the overflow section for the design conditions by indicating where the curvature of the model crest profile should be adjusted to obtain a uniform pressure of approximately minus 5 feet of water along the spillway face. Lower pressures usually occur where the degree of curvature is too great.

To verify the magnitude and uniformity of the pressures on the computed profile would require tests on a model embodying that particular crest shape. However, the observed pressures on the Hungry Horse model tend to confirm the fact that the observed and computed pressures should agree.

LIMITATIONS ON APPLICATION OF RESULTS

Certain limitations should be recognized when applying the experimental results to determine the coefficient of discharge and profile of a morning-glory spillway. The test data were obtained from a circular weir in which the water fell freely through the atmosphere or a partial vacuum. Thus, the upper nappe surface was subject to atmospheric pressure in all tests, while the lower nappe surface was subject to either atmospheric pressure or a partial vacuum depending on the test set-up. Therefore, the head producing the discharge was the head above the weir plus the pressure under the nappe measured in feet of water below atmospheric pressure.

In a morning-glory spillway, the same conditions exist except that the space under the nappe is replaced with concrete. However, when a morning-glory is designed for the submerged condition or with the top of the boil near the crest of the spillway, an additional head is acting on the spillway due to the siphonic action of the column of water in the shaft. This additional head, which does not exist in the circular weir since the jet is surrounded by air, causes a pressure reduction in the shaft and an increase in discharge over the spillway. Therefore, when a morning-glory is designed for near-submerged conditions, similitude between the morning-glory and the circular weir no longer exists. If the shaft is designed to flow partially full, however, flows in the morning-glory and circular weir are similar.

In applying the experimental results from the circular weir to a morning-glory spillway, some means of maintaining the design pressure along the lower nappe surface should be provided to restore similitude between the two flows. The design pressure may be maintained by several methods, among which are the following:

(a) Design the morning-glory with a small $\frac{Hs}{R}$ ratio such that the shaft never flows full.

(b) Place a constriction in the shaft at any point below the boil to maintain the design pressure under the nappe at the boil.

(c) Provide air vents under the nappe at the boil to relieve the suction head due to the shaft flowing full.

In Hungry Horse Dam, air was supplied to the lower nappe surface by means of several air vents placed under the lip of the ring gate. In addition, a 6- by 6-foot air vent was placed in the crown of the vertical bend connecting the shaft with the inclined tunnel. Model tests on Hungry Horse Dam Spillway showed that pressures lower than those indicated in Figure 16 were observed when the above air vents were closed.

Additional research work is required to economically design a submerged morning-glory spillway with a pressure-controlled profile. However, if the above limitations are recognized and means are provided to deal with them, the experimental results should prove helpful in designing a morning-glory spillway.

BIBLIOGRAPHY

1. C. S. Camp and J. W. Howe, "Tests of Circular Weirs," Civil Engineering for April 1939, Vol. 9, No. 4, pages 247-48, New York, American Society of Civil Engineers.

2. H. J. F. Gourley, "Experiments on the Flow of Water Over Sharp-Edged Circular Weirs," Minutes of Proceedings of the Institution of Civil Engineers, Vol. CLXXXIV, pages 297-317. Published in 1911 by The Institution, London, England.

3. R. B. duPont, "Determination of the Under Nappe over a Sharp Crested Weir, Circular in Plan with Radial Approach." Thesis submitted to Case School of Applied Science, Cleveland, Ohio, in 1937.

4. Hunter Rouse, "Engineering Hydraulics," Chapter III by J. W. Howe, page 214, published by John Wiley and Sons, New York, 1950.

5. Bureau of Reclamation, "Studies of Crests for Overfall Dams," Part VI, Bulletin 3, Boulder Canyon Project Final Reports, Denver, Colorado, 1948.